Naval Research Laboratory
Stennis Space Center, MS 39529-5004

NRL/FR/7176--95-9628

Research Ambient Noise DIrectionality (RANDI) 3.1 Physics Description

J. ERNEST BREEDING, JR.
LISA A. PFLUG

Ocean Acoustics Branch
Acoustics Division

MARSHALL BRADLEY
MELANIE HEBERT WALROD
WALTON MCBRIDE

Planning Systems Incorporated
Slidell, LA 70458

August 8, 1996

DISCLAIMER NOTICE

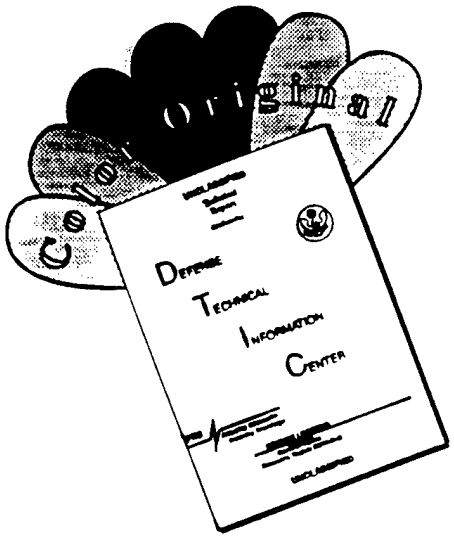

THIS DOCUMENT IS BEST QUALITY AVAILABLE. THE COPY FURNISHED TO DTIC CONTAINED A SIGNIFICANT NUMBER OF COLOR PAGES WHICH DO NOT REPRODUCE LEGIBLY ON BLACK AND WHITE MICROFICHE.

REPORT DOCUMENTATION PAGE

Form Approved
OBM No. 0704-0188

1. AGENCY USE ONLY *(Leave blank)*	2. REPORT DATE	3. REPORT TYPE AND DATES COVERED
	August 8, 1996	Final

4. TITLE AND SUBTITLE

Research Ambient Noise DIrectionality (RANDI 3.1) Physics Description

5. FUNDING NUMBERS

Job Order No. 5716700A6
Program Element No. 0602435N
Project No. 71-5354-B5
Task No.
Accession No.

6. AUTHOR(S)

J. Ernest Breeding, Jr., Lisa A. Pflug, Marshall Bradley*, Melanie Hebert Walrod*, and Walton McBride*

7. PERFORMING ORGANIZATION NAME(S) AND ADDRESS(ES)

Naval Research Laboratory
Acoustics Division
Stennis Space Center, MS 39529-5004

8. PERFORMING ORGANIZATION REPORT NUMBER

NRL/FR/7176--95-9628

9. SPONSORING/MONITORING AGENCY NAME(S) AND ADDRESS(ES)

Office of Naval Research Detachment
Stennis Space Center, MS 39529

10. SPONSORING/MONITORING AGENCY REPORT NUMBER

11. SUPPLEMENTARY NOTES

*Planning Systems Incorporated, 115 Christian Lane, Slidell, LA 70458

12a. DISTRIBUTION/AVAILABILITY STATEMENT

Approved for public release; distribution unlimited.

12b. DISTRIBUTION CODE

13. ABSTRACT *(Maximum 200 words)*

A description is presented of the physics behind the Research Ambient Noise DIrectionality (RANDI) model version 3.1. The RANDI 3.1 model can be used to predict ambient acoustical noise levels and directionalities at low- to midfrequencies for shallow- and deep-water environments. Ambient noise due to shipping, wind, flow noise, and system noise are considered. Shipping noise can be calculated for highly variable environments and is done using either a finite element or split-step parabolic equation. Local wind noise is computed based on the range-independent theory of Kuperman-Ingenito, including both discrete (normal modes) and continuous spectra. Navy-Standard and historical data bases are used to describe the environment. Sample outputs are presented to illustrate products of the model.

14. SUBJECT TERMS

ambient noise, shipping noise, wind noise, shallow-water acoustics, parabolic equation, array response

15. NUMBER OF PAGES

35

16. PRICE CODE

17. SECURITY CLASSIFICATION OF REPORT	18. SECURITY CLASSIFICATION OF THIS PAGE	19. SECURITY CLASSIFICATION OF ABSTRACT	20. LIMITATION OF ABSTRACT
Unclassified	Unclassified	Unclassified	Same as report

CONTENTS

RESEARCH AMBIENT NOISE DIRECTIONALITY (RANDI) 3.1 PHYSICS DESCRIPTION

1.0 INTRODUCTION

The purpose of this report is to present a description of the physics underlying the Research Ambient Noise DIrectionality noise model version 3.1, hereafter referred to as RANDI 3.1. A companion report, the *RANDI 3.1 Users Guide* (Breeding et al. 1994), has been prepared for those who plan to use this model.

The RANDI 3.1 noise model is designed to predict the response of low- to mid-frequency sonar receivers to the ocean acoustic noise field in locations with highly variable surrounding bathymetry and range-dependent sound speed structure. Such environments are typical of the complex oceanographic areas found in shallow water and coastal areas. However, the RANDI 3.1 model can be applied equally well in deep-water areas. In RANDI 3.1, state-of-the-art acoustic propagation models, computational algorithms, and geographic environmental data bases are combined into a single product.

The RANDI 3.1 model is based on the Research Ambient Noise DIrectionality II (RANDI II) model developed at the SACLANT Undersea Research Centre by Hamson and Wagstaff (1983). The RANDI II model is an ambient noise model that predicts noise levels and directionalities for user-specified environmental and shipping conditions using adiabatic mode theory to propagate energy from individual ships to a receiver array. The array response for each ship is calculated by summing the complex pressure due to individual modes at each hydrophone in the receiver array, followed by either coherent or incoherent summation across modes.

The RANDI II model suffered from computational limitations centered around the use of normal mode theory, making it difficult to use the model in deep water where the number of propagating modes is large or in areas with rapid oceanographic or bathymetric changes, such as found in shallow water. The RANDI 3.1 model overcomes these difficulties by using parabolic equation (PE) propagation loss models to propagate energy from individual ships to the receiver array. Currently, RANDI 3.1 incorporates two PE models: (1) finite element PE (FEPE) and (2) the Navy-Standard PE (NSPE), also referred to as the split-step PE (SSPE). The SSPE model (Hardin and Tappert 1973) is a solution to the parabolic equation that involves a marching type Fourier transform. The SSPE has a relatively wide angle capability with up to 40° half-beamwidth. The FEPE model (Collins 1988, 1989) is based on a Pade series expansion of the depth-dependent part of the parabolic equation. The FEPE was developed in an effort to handle propagation angles approaching 90°. The use of PE propagation codes in RANDI 3.1 greatly extends the frequency range and the range of oceanographic conditions for which valid noise predictions can be made.

The RANDI 3.1 model computes the shipping noise complex pressure by one of three propagation methods. These are the rigorous method, the radial accumulation method, and the high-resolution radial accumulation method. The rigorous method executes the propagation model, either FEPE or

SSPE, from each ship to the receiver. The radial accumulation method discretizes the azimuthal direction into radials and executes the propagation model from the maximum ship range of each radial to the receiver, accumulating ships as it marches inward. The high-resolution radial accumulation method, in addition to executing the radial accumulation method, computes the complex pressures at each hydrophone for each ship instead of for each radial. The radial accumulation method and the high-resolution radial method are computed using only the FEPE model.

In RANDI 3.1, as well as RANDI II, local wind noise is estimated using a wave theory model developed by Kuperman and Ingenito (1980). A cross spectral density matrix is determined for all hydrophones in the receiver array.

The RANDI 3.1 model is fully interfaced to supporting geographical environmental data bases of bathymetry, sound speed, bottom properties, shipping, and wind speed. The model extracts environmental information from Navy-Standard data bases including Earth TOPOgraphy 5 (ETOPO5) and Digital Bathymetry Data Base Confidential (DBDBC) for bathymetry; the Historical Ocean Profiles (HOP), the Provinced Generalized Digital Environmental Model (Provinced GDEM), and the High Resolution Shallow Water Sound Speed (SWSS) data bases for sound speed profiles; and the Low Frequency Bottom Loss (LFBL) and Consolidated Bottom Loss Upgrade (BLUG) data bases for bottom parameters. Shipping information is obtained from the Historical Interim Temporal Shipping (HITS) 3.0 and 3.1 data bases, and wind speed from the Historical Wind Speed (HWS) data base. The RANDI 3.1 model also allows for a variety of array types, beamforming options, and output displays.

The shipping noise sources are described in Sec. 2.0 and the environmental data bases are described in Sec. 3.0. In Sec. 4.0, the shipping noise propagation models are explained and the wind noise model is presented in Sec. 5.0. Noise predictions that are independent of the receiver are discussed in Sec. 6.0, while noise predictions that depend upon the receiver array are found in Sec. 7.0.

2.0 SHIPPING NOISE SOURCES

By far, the major component of the total low-frequency (<500 Hz) ambient noise field is the noise generated by ship traffic. Even very distant shipping can be the dominant noise near the horizontal at a receiver array if there is a shoaling sound channel axis or downslope conversion (Wagstaff 1981). Before it is possible to determine the noise due to shipping at a receiver, it is necessary to determine where the ships are located. Each ship is then assigned a heading and source level, as is explained below.

2.1 Estimation of Ship Locations and Headings from HITS

The most extensive data bases of shipping available are the Historical Temporal Shipping (HITS 3.0 and 3.1) data bases (Molinelli 1990; Naval Oceanographic Office 1993; Barnes 1995), which contain shipping densities. These data bases have been incorporated into the RANDI 3.1 model. However, the RANDI 3.1 model requires discrete ship locations to calculate shipping noise, so the densities are converted to discrete locations.

The HITS data bases provide the shipping density for each 1° grid. The densities contain the expected number of ships within each grid for a month, season, or year. Five types of ships are identified according to size: merchant ships, tankers, large tankers, super tankers, and fishing vessels. The fishing vessel densities are given in the HITS 3.0 data base, and they are averaged

annually and for the winter and summer seasons. The densities for the merchant ships, tankers, large tankers, and super tankers are listed in the HITS 3.1 data base, and they are averaged seasonally, monthly, and yearly. Both data bases are unclassified. Figure 1 gives an example of the shipping densities extracted within approximately 3000 km of a receiver array located in the East China Sea outside the Korea Strait at 31° N, 127° E. The densities shown are the sum of densities for the five individual ship classes included in the HITS data bases. Densities for each ship class can also be extracted. For example, Fig. 2 depicts the shipping densities for fishing vessels in this area.

For a given ship type, the shipping densities for a region are used to compute the discrete number of ships for each 1° grid. This is done using a Poisson random distribution function with the extracted ship density as the mean. The Poisson equation is

$$r < \sum_{k=1}^{ships} \frac{e^{-\mu}\mu^{k}}{k!}, \tag{1}$$

where r is a uniformly distributed random number between 0.025 and 0.975, μ is the shipping density, and *ships* is the number of discrete ships. The above equation is solved with the condition *ships* = 0 if $r < e^{-\mu}$. The random number r is confined to the range [0.025, 0.975] rather than [0,1] to prevent the noise field from being dominated by extremes of the Poisson distribution.

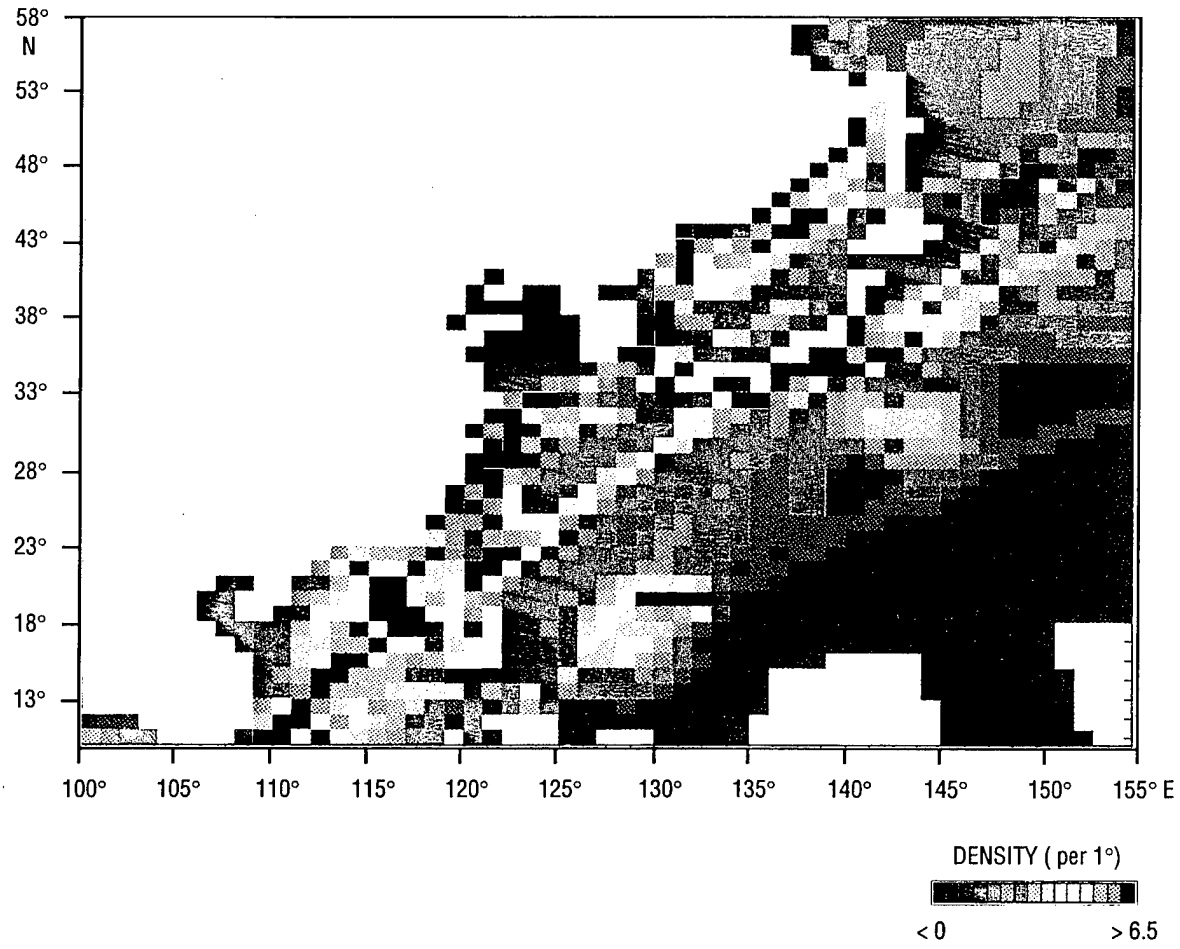

Fig. 1 — HITS 3.1 shipping densities in the East China Sea. All five classes of vessels are included.

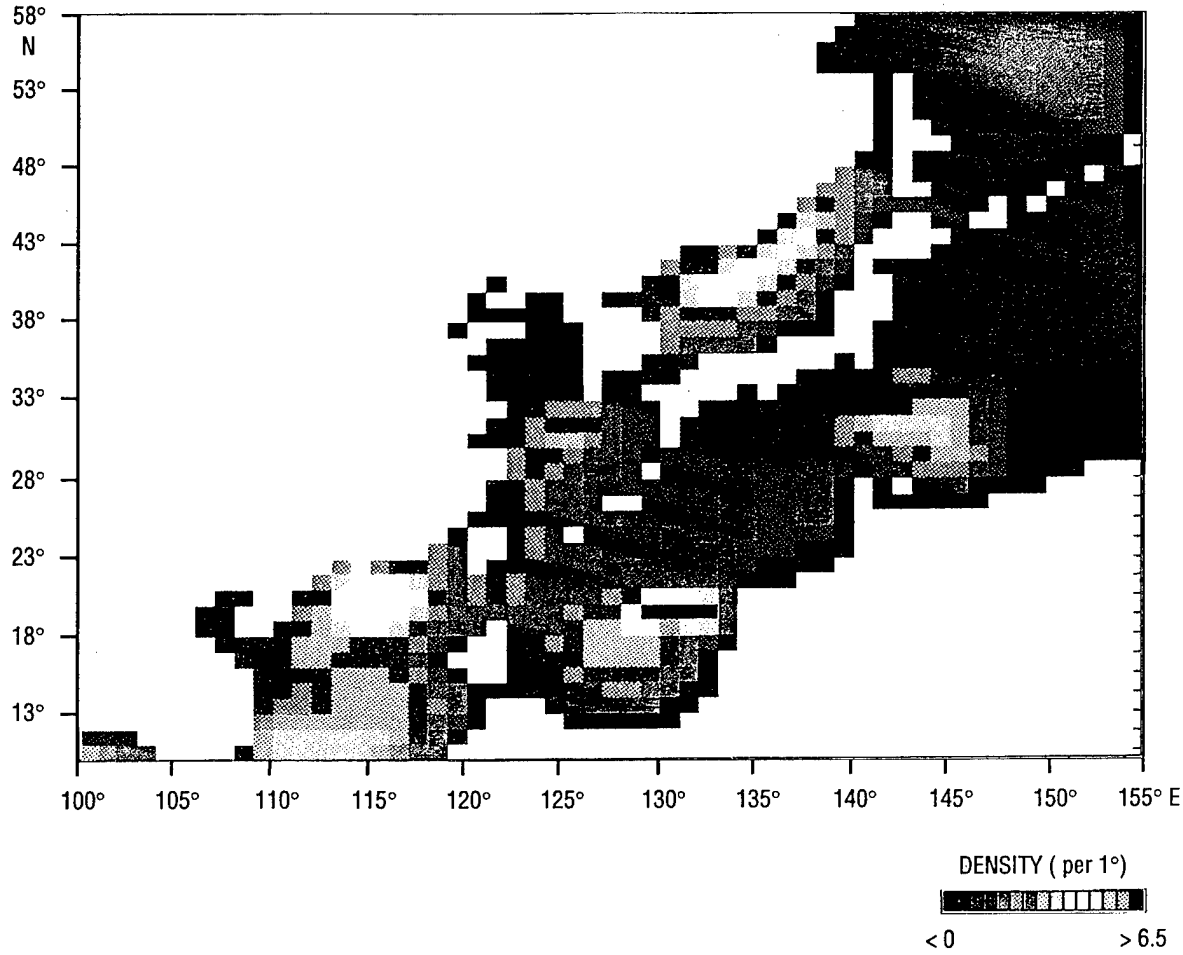

Fig. 2 — HITS 3.1 fishing vessel densities in the East China Sea

For each discrete ship found in the grid, an exact ship location is computed within that grid cell using a uniform distribution function. If a grid cell contains both land and water, the ship location is adjusted so as to not lie on land. Also, the great circle path distance and bearing from the ship location to the receiver is calculated. Figure 3 displays the discrete shipping positions found for the shipping densities shown in Fig. 1. Each ship type is represented by a unique symbol. Ships or radials that are blocked from the receiver by land are ignored in the calculation of noise.

With the exception of fishing vessels, a ship heading is computed for each ship by determining a direction perpendicular to the gradient of the shipping density in the region defined by the grid containing the ship and the grids immediately surrounding this grid. Assuming the gradient points towards the shipping lane, the direction perpendicular to the gradient causes the ship to move parallel to the shipping lane if the ship is dead-reckoned. The fishing vessels are assigned headings generated from a uniform distribution function to simulate their meandering nature.

2.2 Ship Source Levels

The source level of each ship depends upon the length and speed of the ship. A ship length and speed are calculated for each ship by using a uniform random distribution function, but forcing the length and speed to have the limits shown in Table 1.

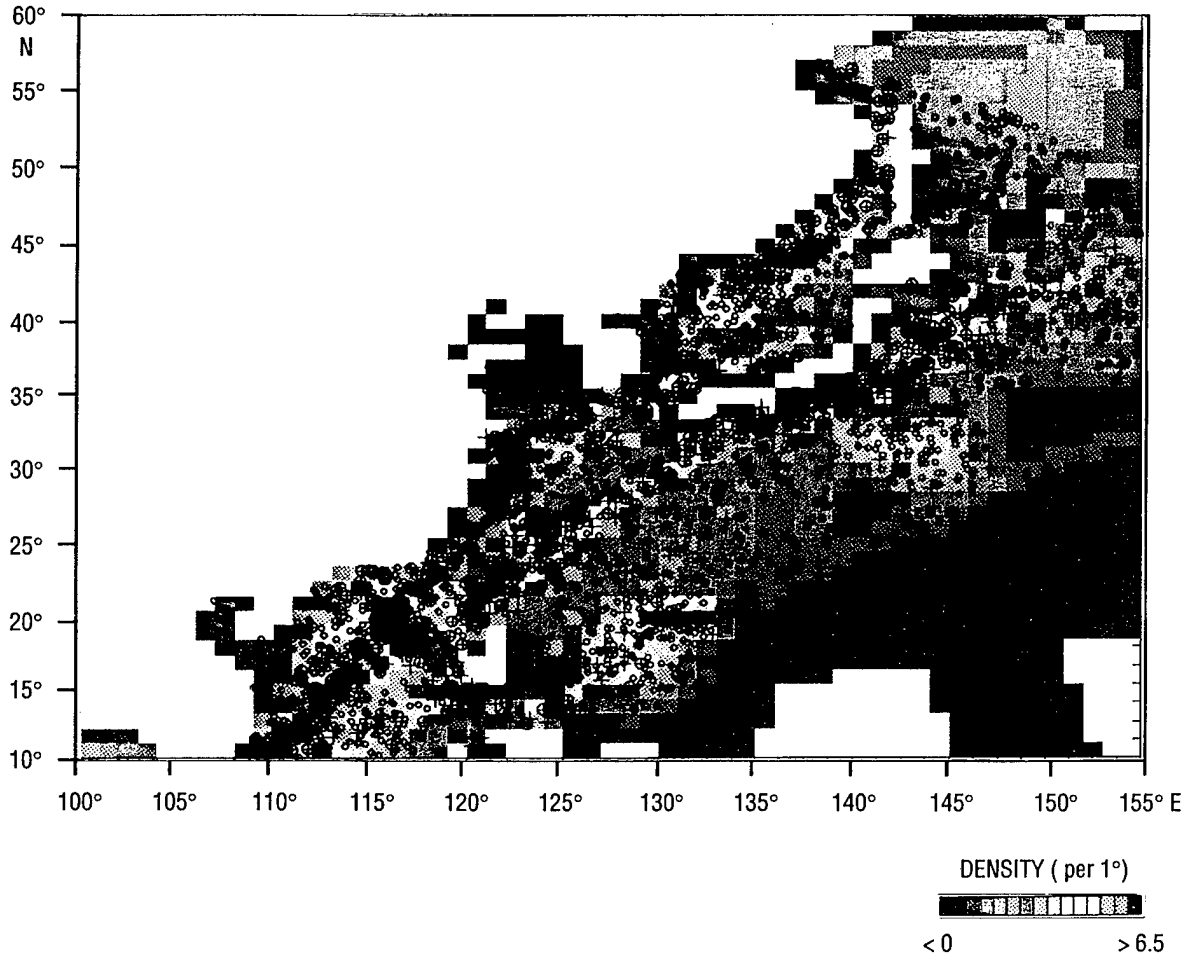

Fig. 3 — Discrete ships in the East China Sea calculated with a Poisson distribution

Table 1 — Length and Speed Limits

SHIP TYPE	LENGTH (ft)	SPEED (kt)
Fishing Vessel	50–150	7–10
Merchant	275–400	10–15
Tanker	400–500	12–16
Large Tanker	500–700	15–18
Super Tanker	800–1200	15–22

The ship source levels are computed by defining an "average" ship as one with a speed of 12 kt and a length of 300 ft. This average ship is assigned a source level of L_{so} dB as a function of frequency. The noise source levels of the actual ships in the model are then calculated, on the basis of their individual speeds and lengths, by the following empirical equation based on Ross (1987).

$$L_s\ (f, v, l_s) = L_{so}\ (f) + 60\ \log(v/12) + 20\ \log(l_s/300) + df * dl + 3.0\,, \qquad (2)$$

where v is the ship's speed in knots and l_s is its length in feet and

$$df = \begin{cases} 0.00 \le f \le 28.40 & df = 8.1 \\ 28.4 < f \le 191.6 & df = 22.3 - 9.77 * \log(f) \end{cases} \tag{3}$$

$$dl = l_s^{1.15} / 3643.0 .$$

For convenience, the equation for $L_{so}(f)$ when $f < 500$ Hz is given by

$$L_{so}(f) = -10 \log(10^{-1.06 \log f - 14.34} + 10^{3.32 \log f - 21.425}) . \tag{4}$$

For values of frequency greater than 500 Hz, $L_{so}(f)$ is given by

$$L_{so}(f) = 173.2 - 18.0 \log(f) . \tag{5}$$

Table 2 shows representative source levels for the different types of ships for several frequencies using average lengths and speeds from Table 1. The source levels are in units of decibels referenced to 1 μ Pa.

Table 2 — Representative Source Levels

SHIP TYPE	10 Hz	25 Hz	50 Hz	100 Hz	300 Hz
Fishing Vessel	142.7	146.5	144.8	136.0	120.0
Merchant Ship	160.9	167.8	162.6	153.5	137.1
Tanker	167.0	170.8	168.6	159.2	141.6
Large Tanker	174.8	178.6	176.0	166.3	149.3
Super Tanker	185.0	188.8	185.4	174.6	156.8

3.0 ENVIRONMENTAL DATA BASES

To determine the amount of energy that propagates from sources to receivers, it is necessary to characterize the different environments with which the waves (rays) interact. The RANDI 3.1 noise model is designed to automatically extract environmental data from a number of data bases along a great circle path from a receiver location to a source. A great circle path is the shortest distance between the receiver and the source on a spherical surface. The great circle path distance (*GCD*) from the receiver to the source is given by

$$GCD = 60 \cos^{-1} (\sin\Theta_s \sin\Theta_r + \cos\Theta_s \cos\Theta_r \cos(\Phi_r - \Phi_s)) , \tag{6}$$

where *GCD* is in nautical miles, Θ_s is the source latitude, Θ_r is the receiver latitude, Φ_s is the source longitude, and Φ_r is the receiver longitude.

Along each great circle path, extraction routines are used to retrieve bathymetry, sound speed, and bottom characteristics at each range segment. The environmental data are extracted whenever the great circle path enters a new grid cell of a particular data base. This section gives a brief description of the individual data bases which RANDI 3.1 accesses to simulate the propagation environment as accurately as possible.

3.1 Bathymetry

The Digital Bathymetry Data Base (DBDB) (Naval Oceanographic Office 1987) contains acoustically measured ocean depths, referenced to a 1500 m/s sound speed. Two DBDB data bases

are incorporated in the RANDI 3.1 model. One version is an unclassified bathymetry data base referred to as ETOPO5, and the other version is a confidential bathymetry data base referred to as DBDBC. Both data bases contain worldwide bathymetry data measured in meters at a 1/12° resolution. Figure 4 shows a view of the ETOPO5 bathymetry found in the East China Sea outside the Korea Strait.

3.2 Sound Speed

The RANDI 3.1 model provides two data bases for the great circle path extractions of sound speed. One of the data bases is the Provinced GDEM data base, which is also known as the HOP data base (Naval Oceanographic Office 1990b). This is a provinced subset of the GDEM data base. The HOP data base contains temperature, salinity, and sound speed profiles at standard depths in the Atlantic Ocean, Pacific Ocean, Indian Ocean, and Mediterranean Sea. The standard depths are 0, 10, 20, 30, 50, 75, 100, 125, 150, 200, 250, 300, 400, 500, 600, 700, 800, 900, 1000, 1100, 1200, 1300, 1400, 1500, 1750, 2000, 2500, 3000, 4000, 5000, 6000, 7000, 8000, and 9000 m. The HOP data base is unclassified, and the data base profiles are seasonal with a resolution of 1/2°.

The second data base provided in RANDI 3.1 is the SWSS data base, and it describes the seasonal temperatures and salinity profiles in shallow water at the standard depths. This data base is detailed in Crout (1991) and was developed by both the Office of Naval Research and Air

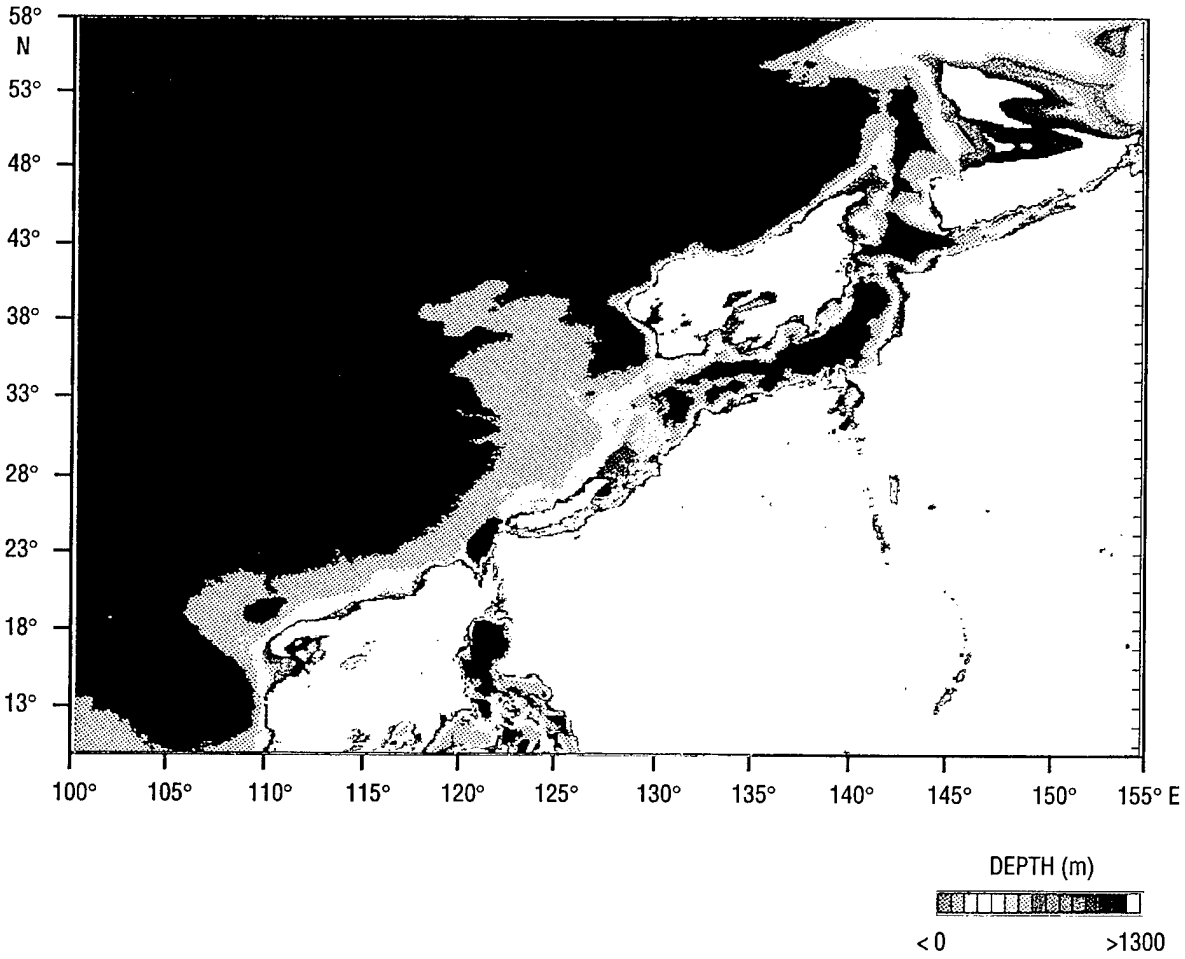

Fig. 4 — Bathymetry in the East China Sea as extracted from the ETOPO5 data base

Defense Initiative. The SWSS data base was developed using the GDEM and Master Oceanographic Observation Data Set data bases in computing the shallow-water profiles for depths between 50 to 500 m. The purpose of the SWSS data base is to allow a smooth transition between the GDEM data base profiles and shallow-water profiles. The SWSS data base has a 1/12° resolution, is seasonal, and unclassified. The coverage is Northern Hemisphere shallow-water regions, excluding the Arctic region.

An example of sound profiles extracted for a tract near the Pacific Coast of the United States is shown in Fig. 5. The bathymetry and the sound channel axis are also shown.

3.3 Bottom Characteristics

The bottom characteristics data bases incorporated in the RANDI 3.1 model include the LFBL and Consolidated BLUG data bases. The LFBL data base is described by the Naval Oceanographic Office (1990) and by Spofford et al. (1983). This data base contains the acoustic properties of the ocean sediment and the sediment thickness at low frequencies (50 to 1600 Hz). In the data base, the ocean is divided into geographical areas that are homogeneous in sediment and composition type. These provinces point to the geoacoustic parameters which provide the BLUG geoacoustic

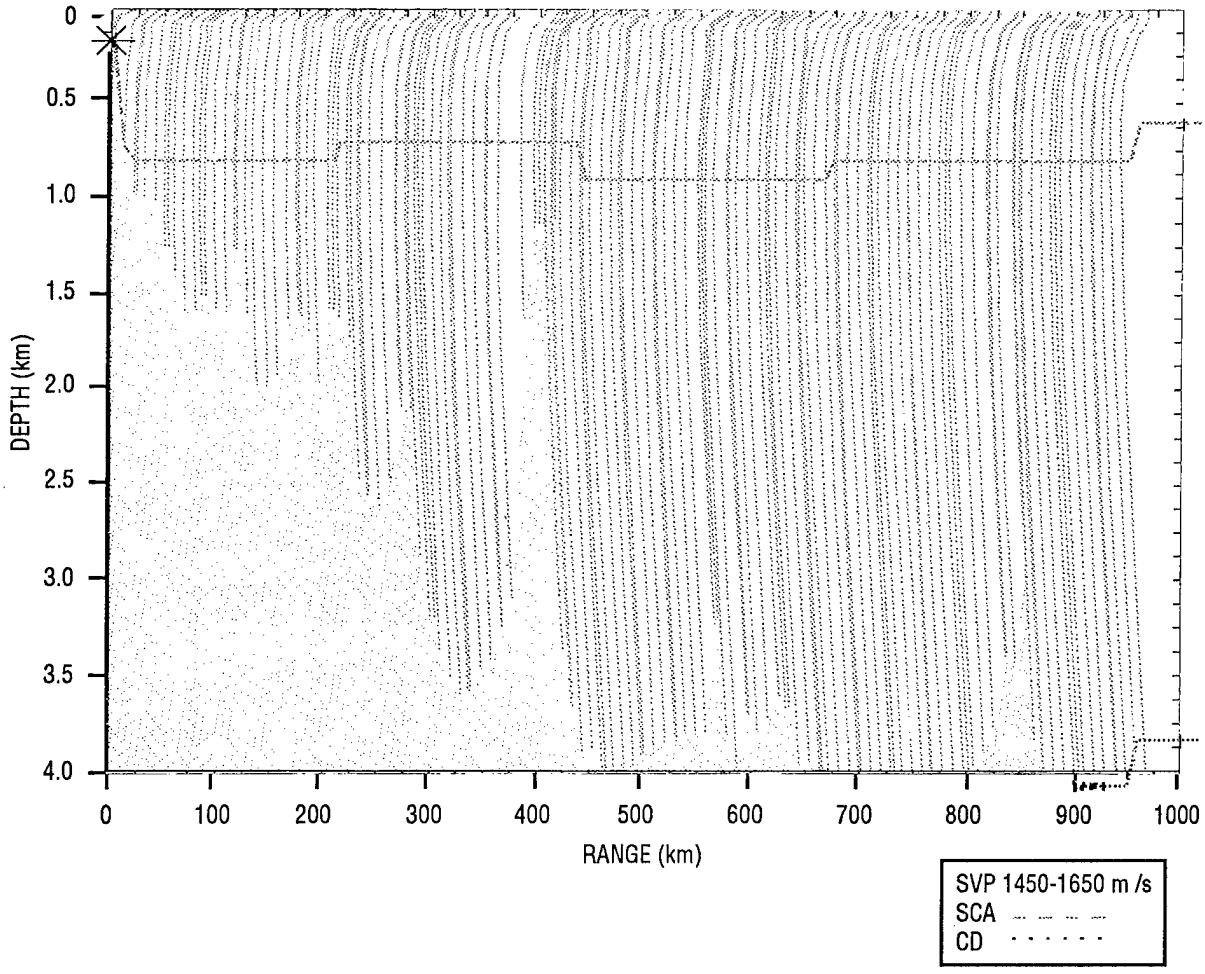

Fig. 5 — Bathymetry and sound speed profiles for a tract near the Pacific Coast of the United States

profile. The geoacoustic parameters describe the sound interaction with the seafloor, density, sound speed, attenuation of the fluid layer, surface layer thickness and density, and substrate reflectivity. In addition, for shallow-water provinces, an attenuation exponent is included as a geoacoustic parameter. The LFBL data base is classified and covers the Northern Hemisphere, the Indian Ocean to 50° S, and the South Atlantic Ocean to 50° S at 1/12° intervals.

The Consolidated BLUG data base is an unclassified version of the LFBL data base. The Consolidated BLUG data base contains the same parameters as the LFBL data base with a resolution of 1/12° grid for the Northern Hemisphere to 65° N, the Atlantic Ocean to 70° N, and the Indian Ocean to 10° S.

The geoacoustic parameters contained in both the LFBL and the Consolidated BLUG data bases are listed in Table 3 and are displayed in Fig. 6.

Table 3 — Geoacoustic Parameters

Sediment Thickness (s)
Water/Sediment Sound Speed Ratio (pure number)
Thin Layer Thickness (m)
Thin Layer Density (gm/cc)
Sediment Surface Density (gm/cc)
Initial Sound Speed Gradient in Sediment (1/s)
Sediment Sound Speed Profile Curvature (1/s)
Attenuation at z = 0 (dB/m/kHz)
Attenuation Gradient (dB/m/kHz/m)
Basement Reflection Coefficient (pure number)
Attenuation Exponent for Shallow Water (pure number)
Two-Way Travel Time (s)

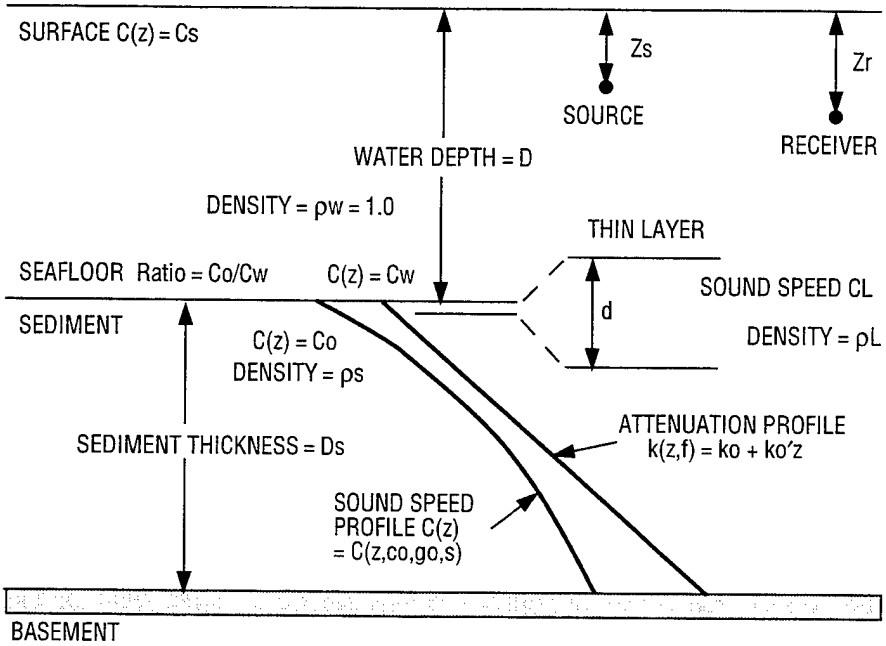

Fig. 6 — Bottom parameters included in the LFBL and consolidated BLUG data bases

Once the bottom characteristics are extracted from a data base they are then converted into a sediment sound speed profile and are used to compute the density and attenuation in the sediment and bottom. A shear sound speed and attenuation are also calculated.

3.4 Wind Speed

The wind source levels are computed in RANDI 3.1 with data extracted from the HWS data base (Naval Oceanographic Office 1989). The HWS data base contains temporal surface statistics taken from marine ships. Included are the number of reports of wind speed and direction, the mean and standard deviation of the wind speed, the percentage of wind direction reports for calm and variable sea states, and the mean wind speed and its wind direction for 45° sectors. The HWS data base covers the Northern Hemisphere and the Southern Hemisphere to 65° S. The resolution is a 1° grid and the temporal resolution is monthly. This data base is unclassified.

4.0 PROPAGATION OF SHIPPING NOISE

Once a source has been located and the source level determined it is necessary to propagate energy to the receiver array. The objective is to calculate the complex pressures at the hydrophones of a receiver array (Sec. 6.0). One way to find the answer is to obtain numerical solutions to the wave equation, which is a second-order differential equation. However, through approximations, it is possible to obtain a parabolic differential equation which is first order, and it is much easier to solve numerically. Two PE methods will be described that lead to a calculation of the pressures at the receiver array. One of the PE models is based on a split-step algorithm and is referred to as the SSPE or NSPE. The other PE model is based on a finite element code, and it is referred to as FEPE.

The environmental data (Sec. 3.0) required for the propagation models are bathymetry, sound speed in the water, sediment, and bottom; and attenuation and density for the sediment and bottom layers. The bottom characteristic data base includes geoacoustic parameters that must be converted to FEPE or SSPE model sediment and bottom inputs.

4.1 The Parabolic Approximation

Underwater acoustic propagation for a monochromatic source is given by the Helmholtz equation, also known as the reduced wave equation. In cylindrical coordinates it can be expressed as

$$\nabla^2 p + k_o^2 \, n^2 \, (r, \phi, z) p = 0 \, , \tag{7}$$

where p is the acoustic pressure, k_o is the wave number given by ω/c_o, with ω being the angular frequency of the source, and c_o is the sound velocity at some reference depth. The index of refraction $n = c/c_o$, where c is a function of the horizontal range r, the depth z, and the azimuthal angle ϕ.

Generally, azimuthal variations of the sound speed are small and can be neglected. In a waveguide such as the ocean, cylindrical spreading occurs, and it can be factored out with the substitution of

$$p(r, z) = u(r, z) e^{ik_o r} / \sqrt{r} \tag{8}$$

into the Helmholtz equation. The phase factor $\exp(ik_o r)$ has also been factored out, leaving an envelope function $u(r, z)$ that obeys the parabolic approximation to the wave equation

$$2ik_o \partial u/\partial r + \partial^2 u/\partial z^2 + k_o^2 (n^2(r, z) - 1)u = 0 . \quad (9)$$

As can be seen from the above equation, the parabolic approximation is a first-order differential equation in the horizontal range r, making it possible to numerically solve it by marching an initial field out in range. Two approaches to solving the parabolic equation are the split-step algorithm SSPE and a finite element technique leading to the FEPE.

4.2 Split-Step PE

The split-step algorithm was the first numerical method applied to the solution of the parabolic equation by Tappert (1974), and it involves a marching-type Fourier transform solution. Since one cannot numerically deal with an infinite transform, a false bottom is added where the envelope u is attenuated. The SSPE used in RANDI 3.1 is a wide-angle (up to 40° half-beamwidth) extension of Tappert's original solution due to Thomson-Chapman (1983), and it has been adopted as the NSPE.

4.2.1 Characteristics of SSPE

In addition to its relatively wide-angle capability, the SSPE is an efficient algorithm to compute. This efficiency comes about through the use of the Fourier transform in marching the solution in range. In addition, the SSPE uses the maximum range step allowed before significant errors are introduced.

The SSPE requires small range steps when large propagation angles are involved. In addition, a uniform depth grid is required with the number of points in that grid confined to a power of 2 for speed in calculating the Fourier transform. Finally, density variations or discontinuities are a special problem, and a "smearing out" of such changes is necessary. For a density discontinuity from ρ_1 to ρ_2 at the depth $z = z_b$, the discontinuity is replaced with the hyperbolic tangent smoother

$$\rho(z) = \rho_1 + 5(\rho_2 - \rho_1)\{1 + \tanh[(z - z_b)/L]\} , \quad (10)$$

where L defines the length of the transition region over which the discontinuity is smoothed, usually chosen such that $k_o L = 2$.

4.2.2 SSPE Inputs from Extracted Bottom Parameters

An advantage of the NSPE model is that it allows the user to input the BLUG parameters (Sec. 3.0) as they are extracted. The values are converted to the necessary bottom inputs, such as sediment and basement sound speed, density, and attenuation. The only input that must be derived is the sediment thickness D_s, which is inferred from the two-way travel time T_2. The relationship between T_2 and D_s is

$$(1/2)T_2 = \int_0^{D_s} c_b(z)^{-1}\, dz, \quad (11)$$

where in BLUG, the sound propagation speed in the bottom $c_b(z)$ is assumed to be of the form

$$c_b(z) = c_0\{(1 + \beta)[1 + 2gz/(c_0(1 + \beta))]^{1/2} - \beta\} , \quad (12)$$

where c_0 is the initial sediment sound speed, g is the sound speed gradient at the water-sediment interface, and β is the sediment sound speed profile curvature factor.

The closed form solution to the above integral is

$$T_2 = 2[(c_D/c_0) + \beta ln(c_D/c_0) - 1]/[g_0(1 + \beta)] . \quad (13)$$

This equation is then solved numerically for c_D. The value of D_s is then determined from the equation for $c_b(z)$. In RANDI 3.1, the value of D_s is not allowed to be greater than 2000 m.

4.3 Finite Element PE

Recently, an FEPE model (Collins 1988, 1989) based on a Pade series expansion of the depth-dependent part of the parabolic equation was developed in an effort to handle propagation angles greater than the 40° half-beamwidth capability of the SSPE. In the FEPE model, the parabolic equation is solved using Galerkin's finite elements method for depth discretization and the Crank-Nicholson method for integration in range. This code is used in RANDI 3.1, and it contains an efficient tridiagonal system solver designed to minimize computation time.

4.3.1 Characteristics of FEPE

The tridiagonal solver is more efficient than the Gaussian elimination method for range-dependent bathymetries. Because the FEPE model does not require a uniform depth grid, density and sound speed discontinuities can be better approximated without a substantial increase in the number of depth grid points as in the SSPE. However, the current FEPE code does not handle variable depth grids. The Pade series approximation to the depth-dependent part of the parabolic equation enables the FEPE to propagate at angles up to 90° half-beamwidth.

Whereas the SSPE can be regarded as automated because of its own selection of range step and depth transform size, the FEPE requires that the user input both range and depth steps. As a general rule, the maximum range increment used should be a half-wavelength, and the maximum depth increment used should be a quarter-wavelength. The increments need to be small enough to adequately model variations in the environment. The FEPE has a choice of starter types including the Gaussian starter, the Green's starter, the homogeneous mode starter, and the image starter.

4.3.2 FEPE Inputs from Extracted Bottom Parameters

It is necessary that the data extracted from the LFBL data base (Sec. 3.0) be converted to values that can be input into the model. As in the SSPE preparation, D_s is calculated using the two-way travel time and the expression for $c_b(z)$ given in Sec. 4.2.2. The sediment sound speed profile is calculated using the equation for $c_b(z)$. The compressional wave velocity in the basement is simply $c_b(D_s)$, where the sediment density is entered as extracted from the data base. The basement density is calculated using the relationship

$$\rho_b = \rho_s (1 + R)/(1 - R) , \quad (14)$$

where ρ_s is the sediment density (from BLUG) and R is the BLUG basement reflection coefficient. The attenuation as a function of depth is calculated from

$$\mu_b (z) = (f/1000)(c_b (z)/f)(k_0 + k_0' z) , \quad (15)$$

where f is the frequency in hertz, $c_b(z)$ is the sediment sound speed at depth z, k_0 is the surface sediment attenuation factor in dB/m/kHz, and k_0' is the attenuation gradient in dB/m/kHz/m.

If a Hamilton type bottom is used in the model, the basement is assumed to be basalt. The compressional wave velocity in the basement is estimated to be 5300 m/s. The density in the sediment is calculated using the expression

$$\rho_d = 1.2 + [(\bar{c}_s - c_b(z_1))/1000]^{1/4}, \tag{16}$$

where

$$\bar{c}_s = \{[c_b(z_1)][c_b(D_s)]\}^{1/2}. \tag{17}$$

The density in the basement is set to 2.7 gm/cm^3.

4.3.3 FEPE Example

An example of the propagation of sound determined by the FEPE propagation model is shown in Fig. 7. The sound is generated by five ships on a slope in the Arabian Sea. The ships are assumed

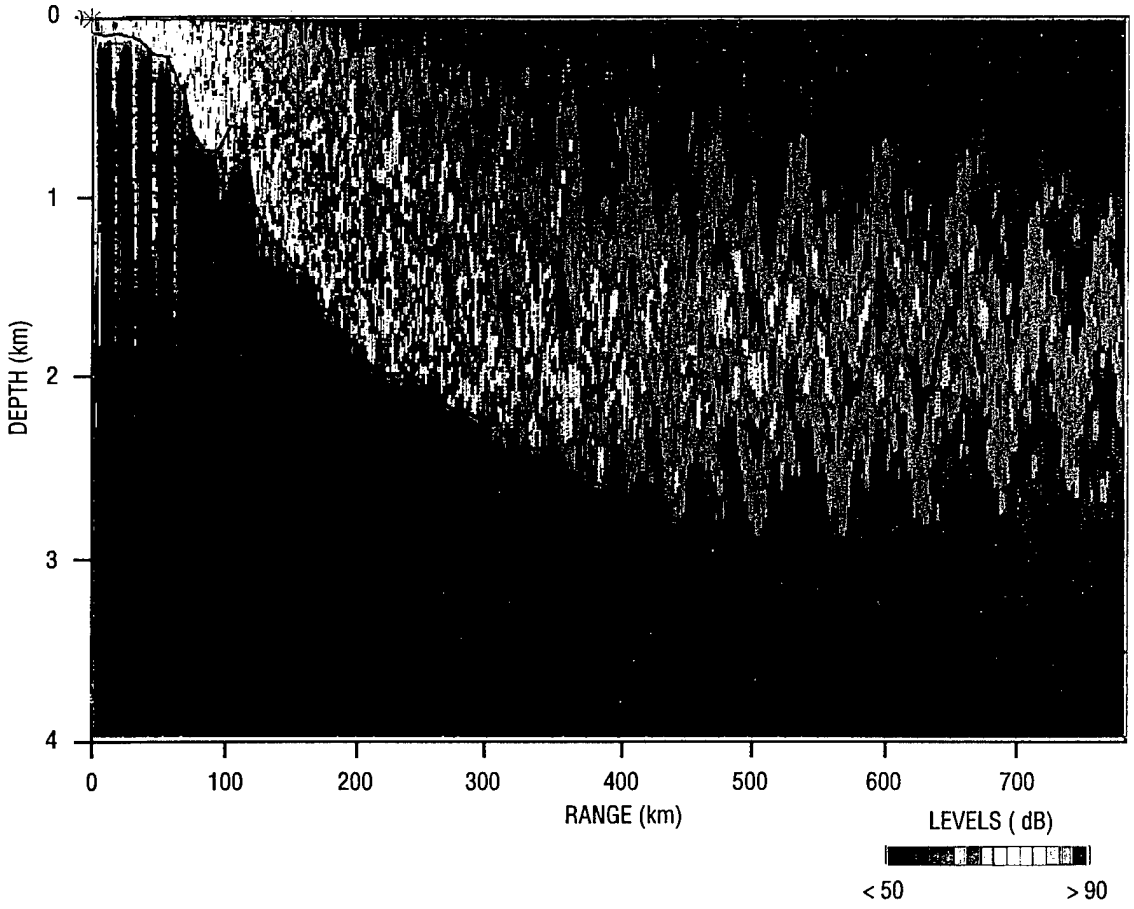

Fig. 7 — Example of downslope noise enhancement as calculated by the FEPE model for five ships on a track in the Arabian Sea

to have equal source levels and are spaced 15 km apart. The location of each source is seen on the left side of the figure. The legend at the bottom right of the figure indicates the signal strength in decibels. In this example, the effects of downslope enhancement are clearly evident. The high-angle energy from the ships has been converted to long-range, refracted-refracted paths cycling at a depth of 1750 m.

4.4 FEPE or SSPE?

In considering the choice of FEPE or SSPE, the user must evaluate the environment being modeled. The FEPE model is best for moderate range dependence, it handles the bottom better, and is accurate up to 90° half-beamwidth. The SSPE model is best for weak range dependence, is accurate up to 40° half-beamwidth, but smoothes density discontinuities.

5.0 WIND NOISE

A major source of ambient noise in the ocean is due to breaking water waves (Felizardo and Melville 1995). Since water waves are primarily generated by the wind, this is referred to as wind noise. Wind noise in the vicinity of the receiver array is computed in RANDI 3.1 using a model due to Kuperman and Ingenito (1980) which was extended by Hamson (1985) to include a more general treatment of source directionality functions. A brief description of the wind model follows.

5.1 Kuperman-Ingenito Wind Noise Model

The Kuperman-Ingenito wind model is range independent with three horizontal layers. The top layer is the water column, the middle layer is composed of sediments, and the bottom layer is the rest of the ocean bottom extending to infinity. In both the water and sediment layers the sound velocity can vary with depth. In the bottom two layers constant values of density and attenuation are assumed. Since the wind model is range independent, the environmental input information is extracted only at the receiver location.

An infinite layer of sources is assumed to exist just below the ocean surface. A complete solution to the wave equation is found which includes a discrete spectrum (normal modes) and a continuous spectrum. The discrete spectrum results from waves which are totally reflected at the bottom and become trapped in the waveguide created by the layering. The spectrum is discrete since energy is found only for those frequencies where constructive interference occurs in the waveguide. The continuous spectrum occurs since the receiver is close to the source where waves reflect from the bottom at less than the critical angle for total reflection. Using the Kuperman-Ingenito wind model, Hamson (1985) shows that continuous modes can be necessary to accurately model measured data in shallow water, especially if the bottom is soft.

Kuperman and Ingenito (1980) and Hamson (1985) derive expressions to compute the spatial correlation function of the noise between any two points. The discrete mode solution is obtained using the SACLANTCEN Normal Mode Acoustic Propagation Model (Jensen and Ferla 1979) and the continuous field solution is computed using the Fast Field Program (Kutschale 1973). In RANDI 3.1, the wind source levels are determined following Wilson (1983). The source level is a function of the frequency and wind speed. The computed wind noise is obtained as a complex spatial correlation matrix between all the hydrophones in the receiver array.

5.2 Wind Noise Bottom Parameters

The value of the sediment thickness, D_s, is computed based on the two-way travel time in the sediment as described in Sec. 4.2.2. To maintain a reasonable number of modes for the wind noise calculation in RANDI 3.1, D_s is not allowed to be greater than 500 m.

The density in the sediment is calculated using the expression

$$\rho_s = 1.2 + [(\bar{c}_s - c_b(z_1))/1000]^{1/4}, \tag{18}$$

where ρ_s is the sediment density, $c_b(z_1)$ is the sediment sound speed at depth z_1, and

$$\bar{c}_s = \{[c_b(z_1)][c_b(D_s)]\}^{1/2}. \tag{19}$$

The remaining bottom parameters refer to the Hamilton bottom type assuming a basalt basement. Sediment compressional attenuation is 0.38 dB/λ, sediment density is 2.7 gm/cc, basement compressional attenuation is 0.106 dB/λ, basement compressional speed is 5300 m/s, basement shear attenuation is 0.188 dB/λ and basement shear speed is 2680 m/s.

6.0 NOISE PREDICTIONS INDEPENDENT OF RECEIVER

In this section, the prediction of ambient noise due to shipping and the local wind will be considered. Three methods will be described for calculating shipping noise. In addition, examples will be presented of noise predictions which are independent of the receiver array.

In the RANDI 3.1 model, the shipping complex pressures are computed by executing one of the PE propagation models, either the FEPE model or the SSPE model (Sec. 4.0). To begin, the model must have a shipping field defined by ship locations and strengths. The environmental shipping density data bases (HITS 3.0 and 3.1) are used to retrieve the shipping densities, and these densities are converted to discrete ship locations. Source levels are assigned depending on the class of ship (Sec. 2.0). The environmental data required for the propagation models are bathymetry; sound speed in the water, sediment, and bottom; and attenuation and density for the sediment and bottom layers (Sec. 3.0). The bottom characteristic data base includes geoacoustic parameters that must be converted to FEPE or SSPE model sediment and bottom inputs. Bottom parameters derived from Hamilton (1980) (ex. in Sec. 5.2) can also be included in the sediment and bottom inputs (Secs. 3.0 and 4.0).

In considering the choice of FEPE or SSPE models, the user must evaluate the environment being modeled and the location of the sources with respect to the receiver. For example, are the sources near or distant? The SSPE model can produce accurate results and be computationally efficient where the propagation is narrow angle (with respect to the horizontal) and weakly range dependent. However, discontinuities at the water-bottom interface create problems for the SSPE model. For complicated bottom interactions, a small computational grid is required to obtain accurate results, and this can severely reduce the computational efficiency of the algorithm. While the SSPE model is accurate for up to 40° half-beamwidth, the FEPE model is accurate up to 90° half-beamwidth. Therefore, the FEPE model is much more accurate than the SSPE model in predicting the noise of nearby sources. The FEPE is also the more accurate of the two models for range-dependent environments such as found in shallow water. Also, in this situation, the SSPE offers no computational advantage (Jensen et al. 1994; Etter 1991).

6.1 Methods for Calculating Shipping Noise

In RANDI 3.1, three different methods are provided for computing shipping noise. These methods are referred to as the rigorous method, the radial accumulation method, or the high-resolution radial accumulation method. Each method is described below.

6.1.1 Rigorous Method

The simplest and most accurate method of computing shipping noise, which is referred to as the rigorous method, entails running one of the PE models from each ship to the receiver. The complex pressures are saved over a portion of the range-depth mesh which encompasses the receiver. Obviously, this method involves as many PE runs as there are ships, and can be very time-consuming for long ranges and a large number of ships. The number of bathymetric and sound speed profile extractions needed is also proportional to the number of ships.

6.1.2 Radial Accumulation Method

One way to reduce the number of environmental extractions and propagation calculations required is to discretize the azimuth into a number of "pie-slice" sectors which are referred to as radial sectors. This is called the radial accumulation method, and it works only with the FEPE model. As shown in Fig. 8, ships are now assigned to particular radial sectors depending on their locations.

The ship positions in a sector are projected onto a radial selected for the sector, and the FEPE is run from the farthest ship to the receiver, accumulating other ships as it propagates along the selected radial toward the receiver. For the particular radial, the total pressure is given by

$$p_T = u_T e^{ik_0 r_c}/\sqrt{r_c}\,, \tag{20}$$

where r_c is the horizontal range from the farthest ship in that radial sector to the receiver center and

$$u_T = \sum_{n=1}^{ships} L_{sn} u_n \sqrt{r_c / r_n}\, e^{-ik(r_c - r_n)} \tag{21}$$

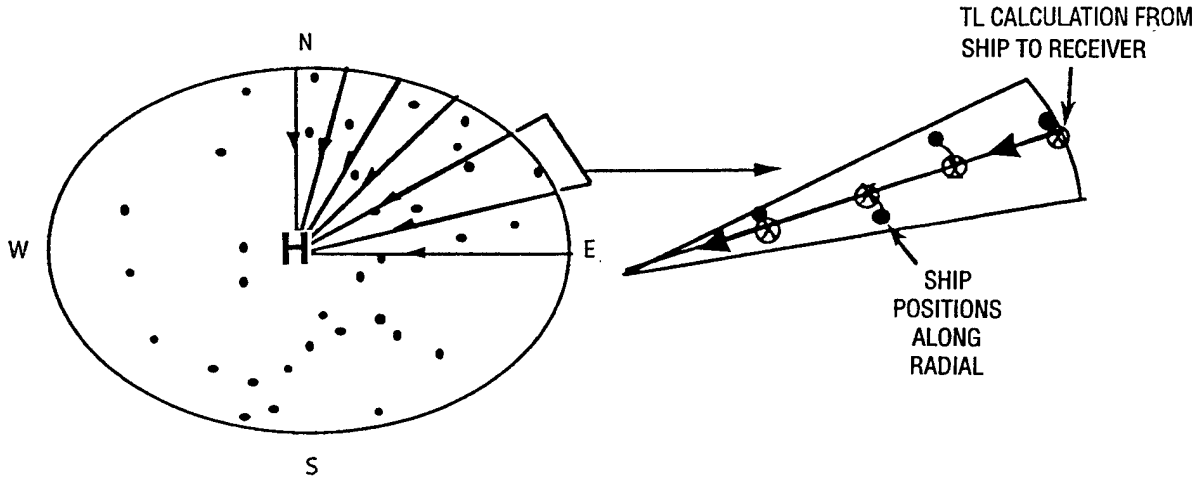

Fig. 8 — Diagram of radial accumulation method for propagation of ships

is the total envelope function obtained by accumulating the ships with source levels L_{sn} as the FEPE propagates. This approximation to the total pressure for a radial is valid only in a local region surrounding the receiver.

The above algorithm is repeated for each radial sector, and it can be seen that the number of FEPE runs has been reduced from the number of ships to the number of radial sectors into which the azimuth has been discretized, saving considerable computing time. However, there is a sacrifice in the accuracy of the results, which decreases with increasing sector size. When dealing with thousands of ships, the rigorous method can become impractical because of the excessive computational time. By comparison, reasonable results can often be obtained with much less computational time by using the radial accumulation method with small sectors.

6.1.3 High-Resolution Radial Accumulation Method

To regain some of the individual ship information lost by the radial accumulation method, RANDI 3.1 also includes an option called the high-resolution radial accumulation method. The ships are accumulated along a radial in a sector just as described in the previous section using the FEPE model. Weighting coefficients are then estimated for each ship in the sector, and these coefficients are used to estimate the complex pressures of the corresponding ships. For a particular sector, the weighting coefficient w_s for a ship s is given by

$$20 \log w_s = SL_s - TL_s , \tag{22}$$

where SL_s is the signal level of ship s at the receiver and TL_s is its transmission loss to the receiver center as approximated by $10 \log r_s$, where r_s is the range from the ship to the center of the receiver. The weighting coefficients are normalized by dividing by the sum of all the weights in the sector, i.e., by the factor

$$\sum_{s=1}^{ships} 10^{(SL_s - 10 \log r_s)/20} . \tag{23}$$

With these weighting coefficients, each ship in a radial sector is assigned the complex pressure

$$p_s = w_s \, p_{radial} , \tag{24}$$

where p_{radial} is the total complex pressure for the radial sector determined by the radial accumulation method. In Sec. 7.1.3, where the interest is beamforming, an adjustment in phase based on a ship's bearing is applied to the pressure at the receiver (hydrophones) for each ship.

Under most circumstances, the high-resolution radial accumulation method would be chosen over the radial accumulation method, since the computational time required for the additional adjustments in complex pressure and phase is negligible. However, the high-resolution adjustments are only approximations, and although tests have shown that the approximations are generally good, for some situations the results may not be sufficiently accurate, or may even be misleading.

6.2 Shipping and Wind Noise

Depending upon which shipping noise calculation option is chosen, the propagation model is then run from the ship (or maximum range of the radial) to the receiver, ignoring ships or radials blocked by land, and saving and accumulating complex pressures at the receiver. The contribution

due to the local wind, if desired, is determined for a range-independent environment (Sec. 5.0) and added to the shipping noise.

The horizontal shipping noise field in the East China Sea near the Korea Strait, as calculated by the three propagation methods, are shown in Figs. 9, 10, and 11 for a frequency of 30 Hz. The maximum ship range is 3000 km, but the number of ships has been randomly thinned to decrease computational time. The receiver is located at 31° N, 127° E. These "spiked" plots represent the horizontal noise field without the array response, i.e., independent of the receiver particulars such as number of hydrophones or hydrophone spacing.

Figure 9 gives the noise field as calculated by the rigorous method. Each spike represents the ship noise contribution with 1° bearing resolution. Nulls in the field are areas of negligible or nonexistent shipping, blockage by land, or a lack of environmental data. It is possible to provide the model with environmental data when they are missing in the included data bases. However, implementation of the data must be performed on a case-by-case basis for a given site and data base.

Figure 10 shows the horizontal shipping noise field as determined by the radial accumulation method. The resolution is equal to the radial sector size which is 5°, corresponding to 72 equally spaced radials. By comparison with Fig. 9 it is seen that the general character of the noise field is preserved. However, a compromise in resolution is evident. At a bearing of about 45°, two spikes are seen close together in Fig. 9. These two spikes become one stronger spike in Fig. 10, since it is not possible to distinguish between bearings in a common sector.

Figure 11 shows the comparable results obtained using the high-resolution radial accumulation method. Noise levels have been assigned to the individual ships using weighting coefficients as described in Sec. 6.1.3. The ships have been assigned their original bearings.

It is interesting to note that 184 ships contributed to the noise field when using the rigorous method, whereas in the radial methods, there were 212 ships contributing to the noise. This happened because in using the rigorous method the propagation path is checked between each ship and the

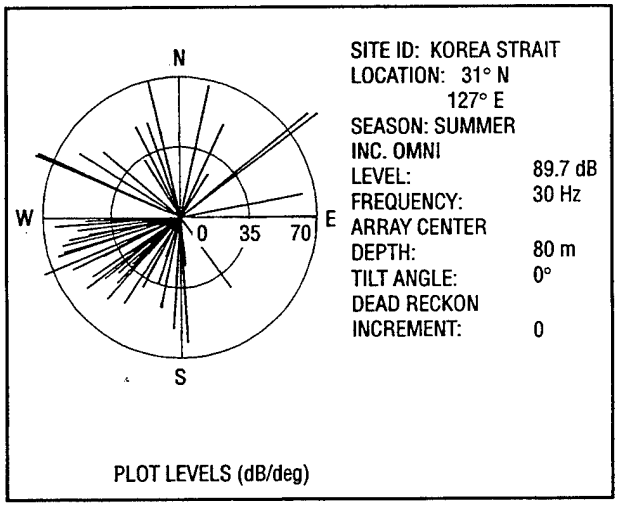

Fig. 9 — Horizontal shipping noise field for 30 Hz in the East China Sea calculated by the rigorous propagation method

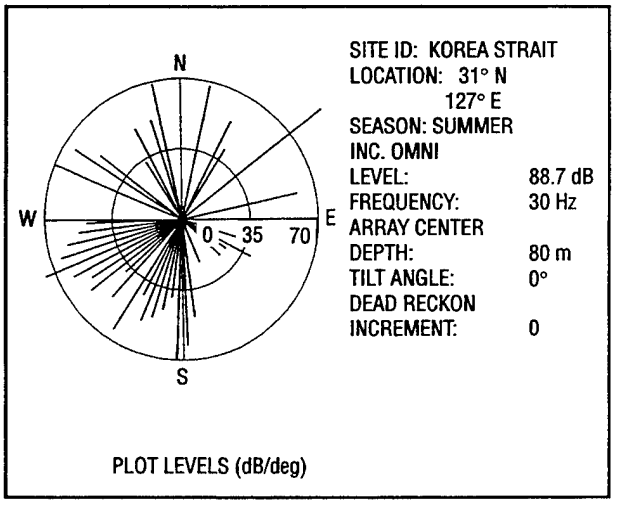

Fig. 10 — Horizontal shipping noise field for 30 Hz in the East China Sea calculated by the radial accumulation propagation method

receiver. A number of ships were obviously found to be blocked from the receiver. In using the radial methods, ships in a sector are only ignored if blockage is found along the propagation radial specified for the given sector.

Figure 12 depicts the horizontal noise field of Fig. 9 with noise from a 10-kt wind included. The omnidirectional level of 50.36 dB, as calculated by the Kuperman-Ingenito model, is divided among 360 1° sectors resulting in a minimum noise level of 24.80 dB for all azimuthal angles.

In RANDI 3.1, the bathymetry and sound speed profiles extracted for use in the propagation model are saved. In addition, the pressure field for a user-selected ship or radial is saved. For example, Fig. 13 contains the environmental information from the 5° radial sector centered on 222.5° used for the calculation of the noise by the three methods. Five ships contribute to the field in this sector. The corresponding pressure field calculated by the FEPE is shown in Fig. 14. Figure 15 depicts the FEPE signal level ($SL - TL$) versus range from the farthest ship to the receiver. The first four ships are located between 0 and 37 km. The fifth ship is located at approximately 458 km, and it produces a noticeable jump in the signal level where its source level is added to the field, as can be observed in Figs. 14 and 15.

6.3 Dead-Reckoning

The RANDI 3.1 model has an option to dead-reckon the ships and compute the shipping noise contributions for each dead-reckoning period. The ships are directed to move along shipping lanes. This is a direction assumed to be perpendicular to the gradient of the shipping density, which is determined by a quadratic fit to twelve 1° grid cells surrounding the ship. Shipping lanes are assumed to be where the greatest concentration of ships are found. Once all the time periods are modeled, an average horizontal noise field is computed by averaging each spatially smoothed noise field calculated for each dead-reckoning period. An example is shown in Fig. 16. The ships surrounding the Korea Strait are dead-reckoned twice over 1-h time periods. The high-resolution radial accumulation method is used to calculate the shipping noise field. The local wind noise contribution (50.36 dB) is added before smoothing and time-averaging is performed.

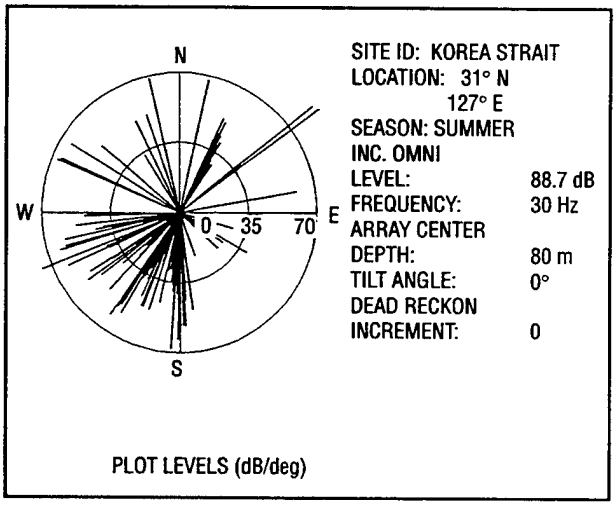

Fig. 11 — Horizontal shipping noise field for 30 Hz in the East China Sea calculated by the high-resolution radial accumulation propagation method

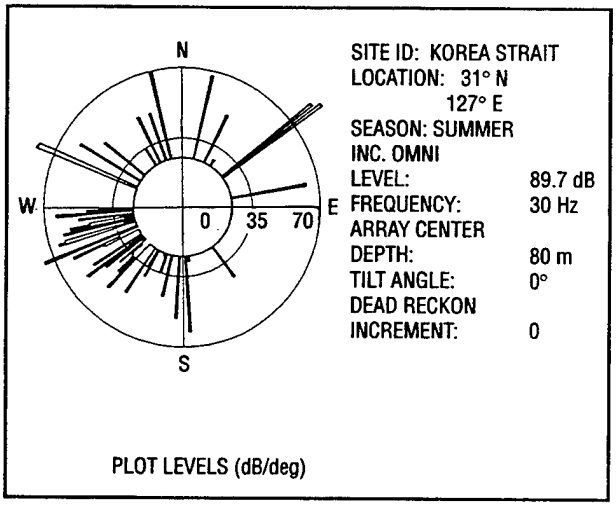

Fig. 12 — Horizontal noise field due to ships and a 10-kt wind

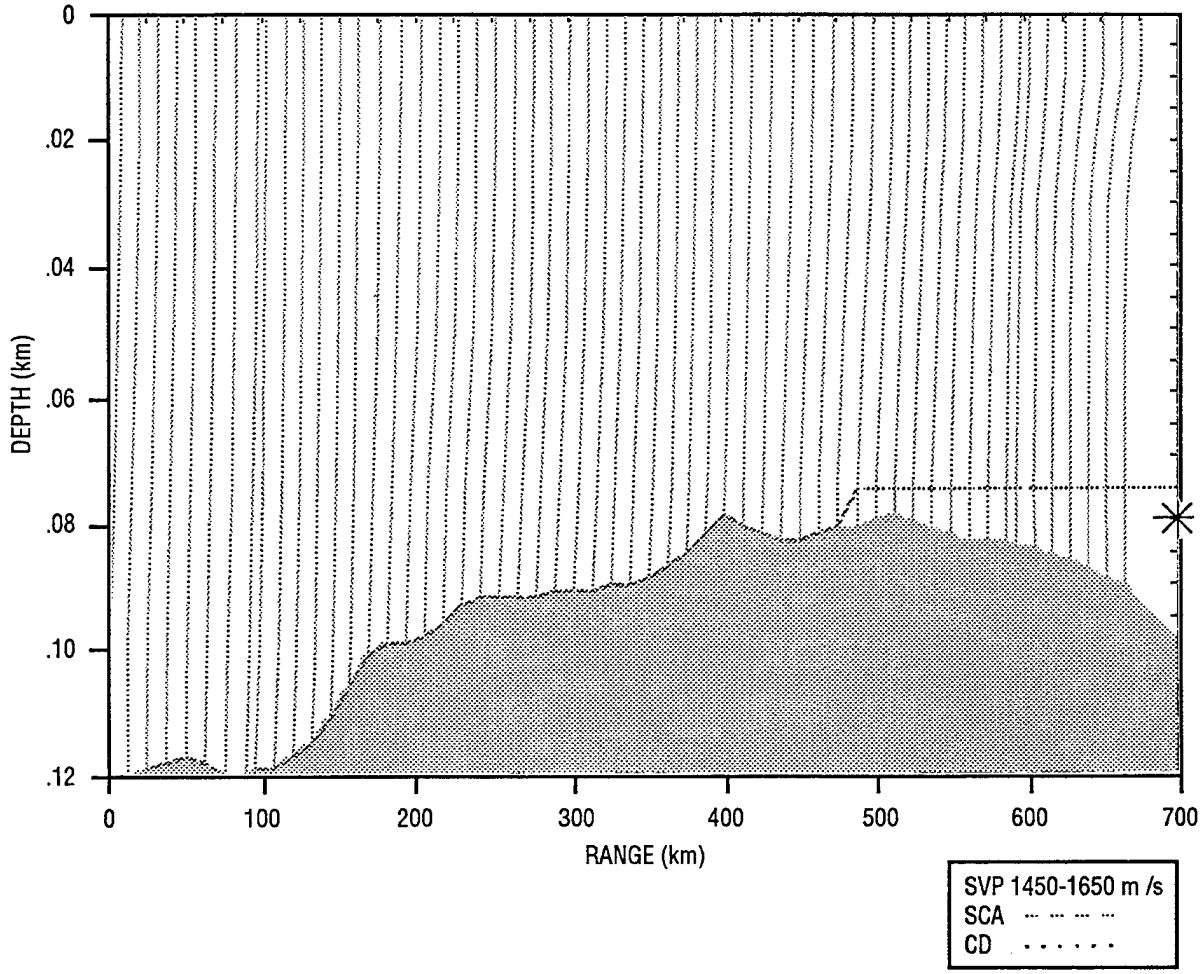

Fig. 13 — Bathymetry and sound speed profiles for the radial sector centered on 222.5°

7.0 NOISE PREDICTIONS DEPENDENT OF RECEIVER

The RANDI 3.1 model produces noise predictions for one of several receiver array types: horizontal, vertical, tilted linear, or volumetric. Linear arrays are assumed to be undeformed and absolute element locations are specified via an array center depth, element spacing, array heading, and tilt angle. Hydrophone locations in volumetric arrays, of which the linear array is a subset, are input in a rigorous manner using a local Cartesian coordinate system at the receiver referenced to the array center depth.

The focus in this section will be on predictions of noise that depend upon the array of sensors (hydrophones) that are used to measure the noise. It should be noted that measurement arrays do not directly measure a noise property such as directionality. Rather, they sample the acoustic pressure at individual hydrophone locations. Beamforming is then used to estimate the directionality of the ambient noise field at a receiver site as a function of arrival angle about the receiver location.

One of the most powerful aspects of the RANDI 3.1 noise model is that it can be used to accurately model the coherent and incoherent beam response of a measurement array to the shipping

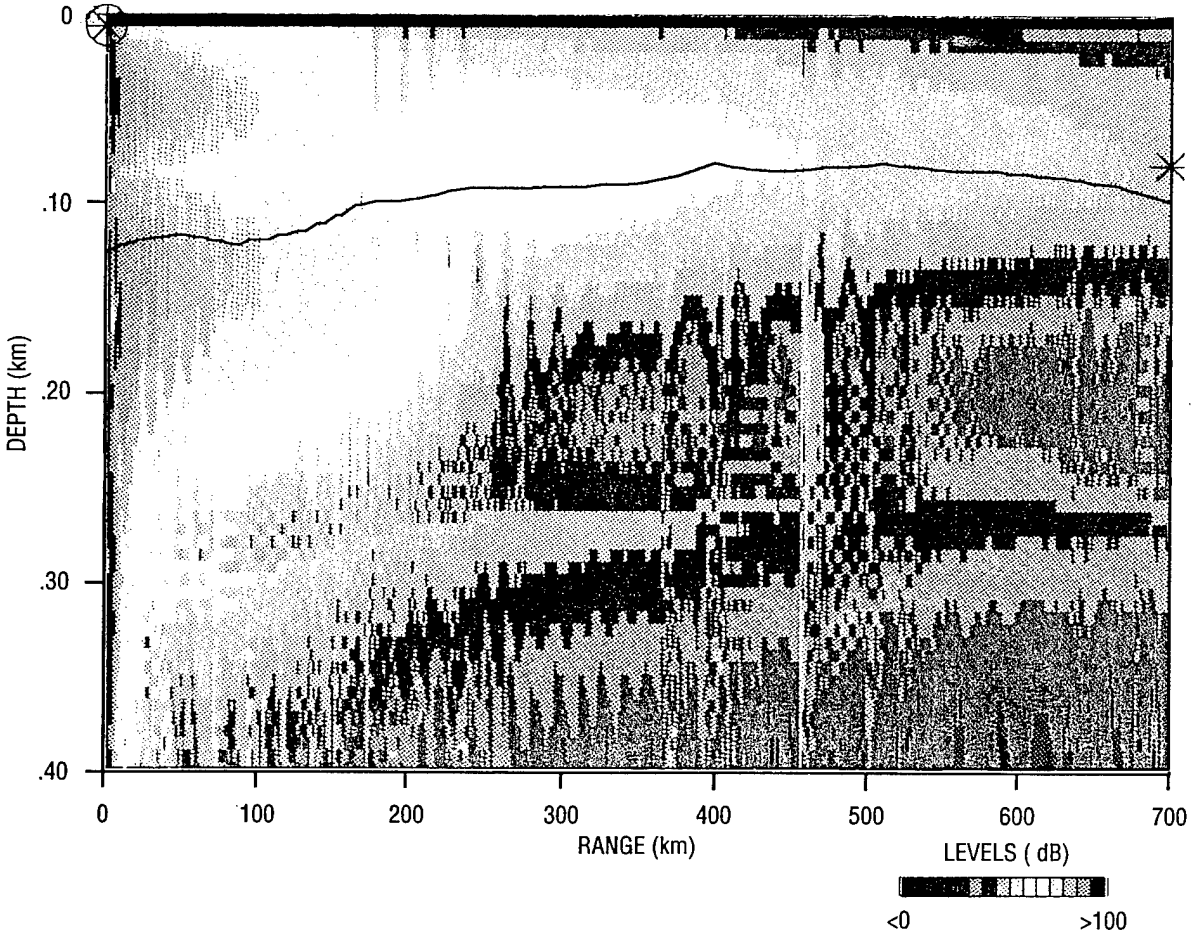

Fig. 14 — FEPE pressure level vs. range and depth for the radial sector centered on 222.5°

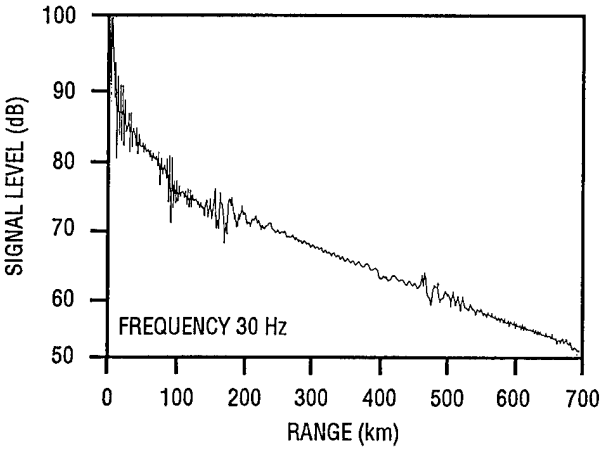

Fig. 15 — FEPE signal level vs. range for the radial sector centered on 222.5°

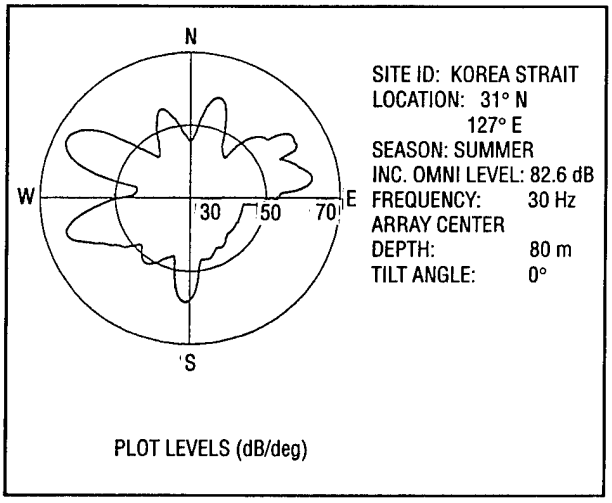

Fig. 16 — Time-averaged horizontal noise field for the East China Sea and two 1-h dead-reckon periods

and wind noise fields at a receiver location. Additionally, it is possible to predict the measurement array responses to system and flow noises.

7.1 Shipping Noise: Complex Pressures

It is necessary to estimate the complex pressures about an array before it is possible to beamform the results. The shipping noise is computed using either the FEPE or the SSPE model (Sec. 4.0) with one of three methods: the rigorous method, the radial accumulation method, or the high-resolution radial accumulation method (Sec. 6.0). Regardless of which method is employed, the values of the envelope function $u(r, z)$, which obeys the parabolic approximation to the wave equation (Sec. 4.1), are saved for range-depth gridpoints in the vicinity of the receiver array of hydrophones. In general, the position of these gridpoints will not coincide with the positions of the array hydrophones, and some type of interpolation will be necessary to obtain the complex pressures at each hydrophone.

7.1.1 Parameters for a Tilted Array

The calculation of the complex pressure at a hydrophone n makes use of the fact that the envelope function $u(r, z)$ calculated by the PE is a slowly varying function of range. As a consequence of this assumption, a linear interpolation between the gridpoints is a good approximation. Toward this aim, both the range and depth coordinates of each hydrophone are calculated.

To be general, it will be assumed that the array is tilted at some angle. The array tilt is specified with the use of a local coordinate system with hydrophone 1 at its origin. The array elevation angle θ is measured from the horizontal with the convention that it is positive in the direction of increasing z, i.e., depth, and its heading ϕ is referenced from north, being positive in the clockwise direction. Given the separation d between hydrophones, the depth of hydrophone n is given by

$$z_n = z_0 + (n-1)d \sin \theta , \tag{25}$$

so that hydrophone 1 is always located at the origin whose depth is z_0, and n runs from 1 to N hydrophones.

The range used to calculate $u(r, z)$ is the distance from each individual ship to the receiver for the rigorous method, and the distance from the farthest ship on the radial to the receiver for the radial accumulation methods. Because the ranges involved in the PE calculations are rather large, a plane wave approximation is used in the estimation of the range to each hydrophone n

$$r_n = r_0 - (n-1)d \cos \theta \cos (\phi_s - \phi) , \tag{26}$$

where r_0 is the range separation between the origin of the local array coordinate system and each ship and ϕ_s is the ship's bearing relative to north as seen in the array coordinate system. For the radial accumulation method, r_0 is the range to the farthest ship in each sector and ϕ_s is the bearing of the sector radial with respect to north, again as observed from the array.

7.1.2 Interpolation of the Complex Pressures

The range-depth gridpoints at which the PE runs produce values for the envelope function $u(r, z)$ and are separated in range by a maximum of a half-wavelength (SSPE and FEPE). The separation in depth is a maximum of a quarter-wavelength for the FEPE model, or a fraction of a

wavelength (determined by the size of the Fourier transform) for the SSPE model. The complex pressures at each hydrophone are obtained by linearly interpolating the values of the envelope $u(r, z)$ over each hydrophone's range and depth and then multiplying the interpolated value of u by a factor which incorporates the phase due the horizontal range and cylindrical spreading. For a hydrophone of index n, the interpolated complex pressure is given by

$$p\left(r_n, z_n\right) = u\left(r_n, z_n\right) e^{ik_0 r_n} / \sqrt{r_n}\,, \tag{27}$$

where r_n is given by the equation in the preceding section, and z_n is the azimuthally independent depth of hydrophone n.

7.1.3 Phase Estimation for the High-Resolution Radial Accumulation Method

Weighting coefficients were obtained in Sec. 6.1.3 to assign pressures to individual ships when the high-resolution radial accumulation method is used. Before it is possible to do beamforming, it is also necessary to apply an adjustment in phase to each ship pressure in a radial sector. Let all bearings be referred to north and be positive in the clockwise direction. For a radial whose median has the bearing ϕ_m, the phase delay between hydrophones for a plane wave reaching a horizontal array with heading ϕ_a is equal to

$$\alpha_{am} = k_0\, d\, \cos\,(\phi_a - \phi_m)\,, \tag{28}$$

where k_0 is the wave number and d is the separation between hydrophones. The actual bearing of ship s, however, is ϕ_s, so that a plane wave emanating from that bearing would suffer a phase delay across this horizontal array equal to

$$\alpha_{as} = k_0\, d\, \cos\,(\phi_a - \phi_s)\,. \tag{29}$$

For a horizontal array, then, the complex pressure assigned to ship s is given by

$$p_s = w_a\, p_{\text{radial}}\; e^{i\Delta\alpha}\,, \tag{30}$$

where $\Delta\alpha = k_0\, d[\cos\,(\phi_a - \phi_s) - \cos\,(\phi_a - \phi_m)]$.

The above result for a horizontal array can easily be generalized to a tilted array, giving the following expression for the complex pressure assigned to ship s

$$p_s = w_a\, p_{\text{radial}}\; e^{i\Delta\alpha\,\cos(\theta_a)}\,, \tag{31}$$

where θ_a is the elevation angle of the array with reference to the horizontal plane.

7.2 Shipping Noise: Noise Directionality

Propagation algorithms based on ray theory lead to straightforward calculations of received energy versus elevation angle, the PE-based algorithms do not. However, this information can be derived from the PE field at the receiver by sampling the water column in the vertical direction and then beamforming to obtain the vertical arrival structure for each ship or radial bearing, depending on whether the rigorous or radial accumulation method is chosen. In what follows, we restrict ourselves to the latter method.

7.2.1 Cosine-Spaced Beams

Beams are steered in the vertical so that they are evenly partitioned in cosine space. If the beam index b runs from 1 to the number of beams B, each beam is steered so that

$$\cos\ \theta_b = 1 - 2(b-1)/B\,, \tag{32}$$

where θ_b is the steering angle as measured from the array heading. The desirable feature of cosine-spaced beams is the fact that they subtend equal areas on the unit sphere. This area is

$$A_{azimuth} = \int_0^{2\pi} \int_{\theta_b}^{\theta_{b+1}} \sin\theta\, d\theta\, d\phi = 2\pi \int_{1-2b/B}^{1-2(b-1)/B} d(\cos\theta) \tag{33}$$

or

$$A_{azimuth} = 4\pi/B\,, \tag{34}$$

which is independent of the beam index b.

For the radial accumulation method, the azimuth is broken up into N_r radials so that the area A_r subtended by the cosine-spaced beams over a radial is

$$A_r = A_{azimuth}/N_r = 4\pi/BN_r\,. \tag{35}$$

7.2.2 Three-Dimensional Directionality

Assume that each cosine-spaced beam is located at the center of each A_r. Then the beam intensity (power per steradian) over an area characterized by the beam index b and the radial index r is

$$I_{br} = \left|p_{br}\right|^2 BN_r/4\pi\,, \tag{36}$$

where p_{br} is the sum of the delayed complex pressures over the array for radial r. The time delay imposed on the complex pressures depends on the beam index b such that

$$\Delta\tau_{n,\,b} = nd\,\cos\,\theta_b/c\,, \tag{37}$$

where n is the hydrophone index, d is the spacing between elements, and c is the reference sound speed.

From the above BN_r values of I_{br}, a panoramic mural of the directionality of the total ambient noise can be created. An example of the noise three-dimensional directionality for the example described in Sec. 6.2 is given in the color plot of Fig. 17. The color scale appears in the bottom right corner of the figure. Each vertical striation of color represents the noise level for one radial.

Noise directionalities for the vertical and horizontal can easily be obtained by appropriate summations of the BN_r values of I_{br}. For example, the vertical directionality of the ambient noise is obtained by computing the noise intensity impinging on the center of the array at a steering angle θ_b from all radials.

Recalling from the discussion above that all cosine-spaced beams subtend an equal area, the vertical beam intensity (power per steradian) is

$$I_b = \sum_r |p_{br}|^2 / A_{azimuth} = \sum_r I_{br} / N_r \ , \tag{38}$$

where the last equality can be verified by substitution of the expression for I_{br} from the previous section. The vertical beam intensity corresponding to a steering angle θ_b is therefore obtained by averaging over the number of radials. An example of the vertical directionality is shown on the right side of Fig. 17. For this example, there is little variability in the vertical direction for a frequency of 30 Hz since the water depth is less than two wavelengths deep. If the receiver array is located farther from the coast at 23° N, 150° E, the three-dimensional and vertical directionalities change as shown in Fig. 18. The increased noise level near horizontal arrival angles in the vertical arrival structure reflects the increased distance between the coastal areas of heavy shipping activity and the receiver array. The omnidirectional noise level is correspondingly decreased from 89.7 dB to 71.7 dB.

The horizontal directionality of the total ambient noise is another easily obtainable quantity from the I_{br} values. To calculate the noise intensity impinging on the center of the array at an

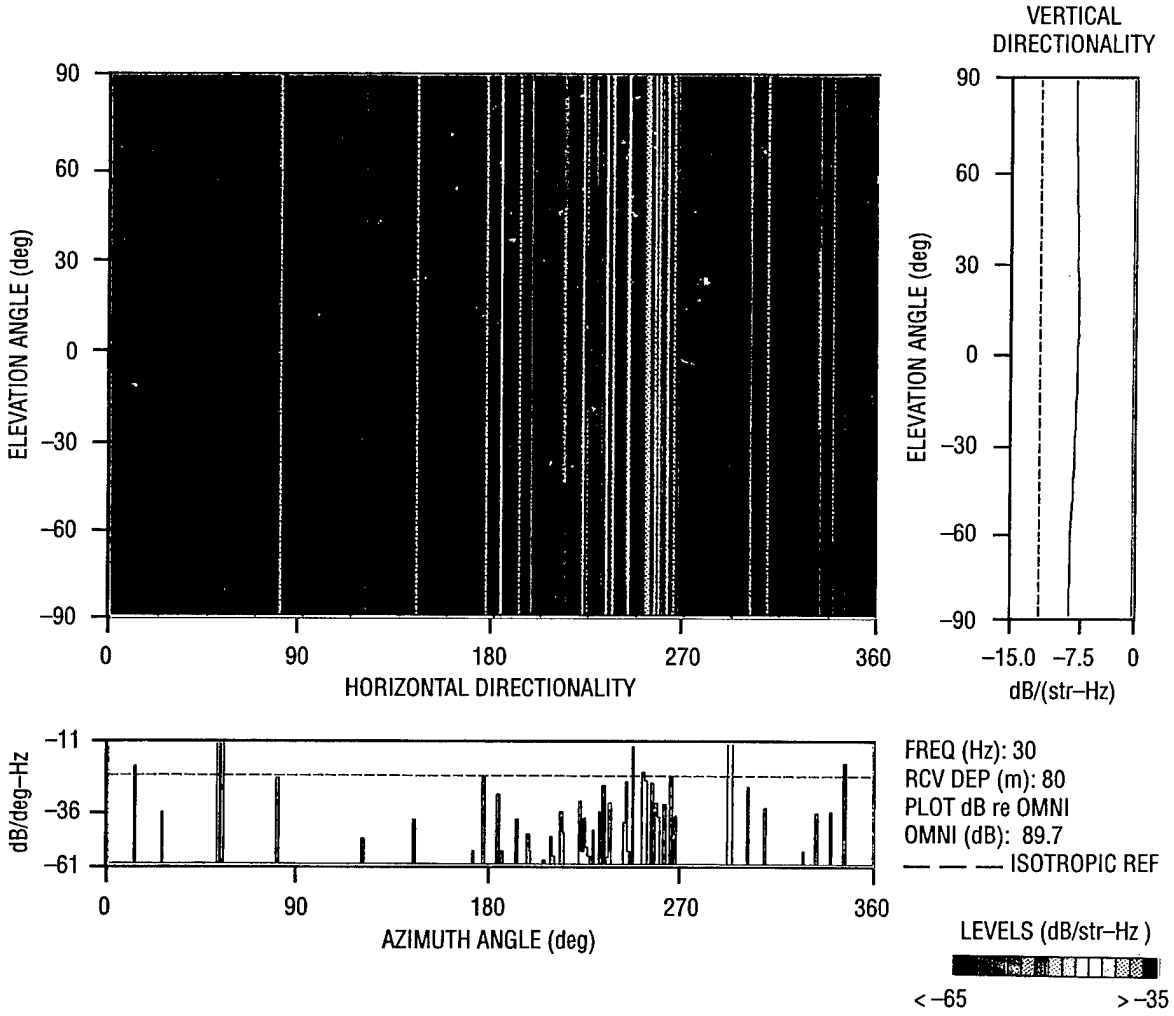

Fig. 17 — Three-dimensional, horizontal, and vertical noise directionalities for a receiver located in the East China Sea near the Korea Strait; ocean depth 99 m

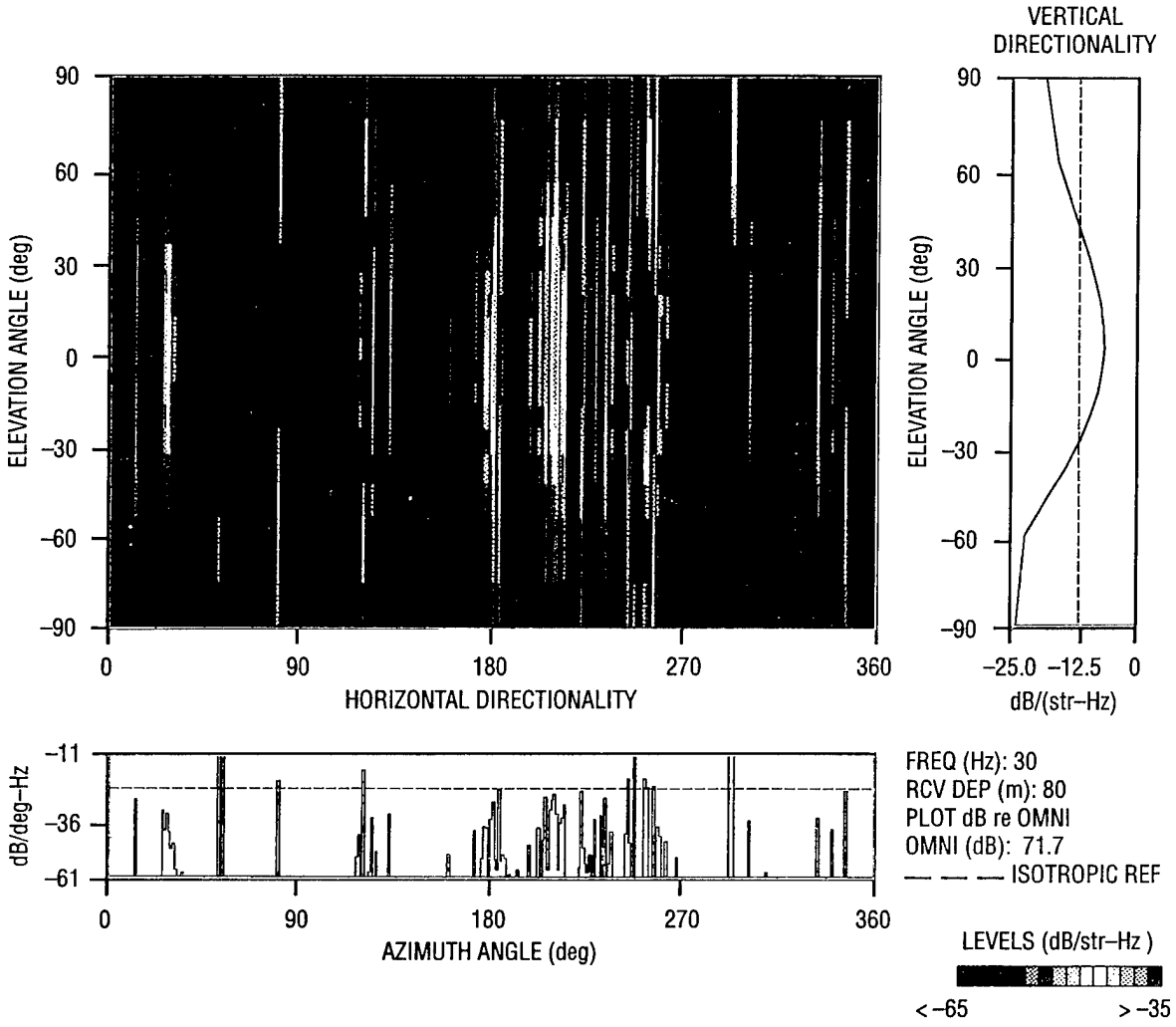

Fig. 18 — Three-dimensional, horizontal, and vertical noise directionalities for a receiver located in deep water outside the East China Sea; ocean depth 5647 m

azimuthal angle ϕ_r, it is necessary to sum the I_{br} over the beam index b for each radial. The area thus subtended is $A_{slice} = 4\pi/N_r$, so that

$$I_r = \sum_b \left| p_{br} \right|^2 / A_{slice} = \sum_b I_{br}/B, \tag{39}$$

where the last equality can again be verified by substitution of the expression for I_{br}. The horizontal beam intensity (power per steradian) over a radial is therefore obtained by averaging over the number of beams.

The horizontal directionality is displayed in terms of power per degree slice instead of beam intensity (power per steradian). No matter what the angular width of the radials, one can always obtain the horizontal beam power over 1° slices by dividing the sum of powers over the beams by the angular width of a radial. Then

$$Power\,(1°) = \sum_b \left| p_{br} \right|^2 N_r / 360 = 4\pi I_r / 360\,. \tag{40}$$

Examples of the horizontal directionality computed by this method are depicted at the bottoms of Figs. 17 and 18. As expected, the azimuthal angles between approximately 180° and 270° contain the highest levels of shipping noise, coming mainly from the East China Sea.

7.3 Spatial Filtering

To perform spatial filtering, RANDI 3.1 includes Discrete Fourier Transform (DFT) and Fast Fourier Transform (FFT) beamformers, each of which is applied in conjunction with one of several standard array shading functions. The noise pressures can be summed either coherently or incoherently during beamforming.

7.3.1 Shading Coefficients

In beamforming noise, it is often desirable to employ shading coefficients. Four beamformer spatial shading options are available in RANDI 3.1. They are unshaded (uniform), Hann, Hamming, and Blackwell. The shading coefficients a_n for these four options are computed as follows:

For an unshaded array,

$$\bar{a}_n = 1 . \tag{41}$$

For a Hann shaded array,

$$\bar{a}_n = 0.5 - 0.5 \cos\frac{2\pi n}{N+1} . \tag{42}$$

For a Hamming shaded array,

$$\bar{a}_n = 0.54 - 0.46 \cos\frac{2\pi (n-1)}{N-1} . \tag{43}$$

For a Blackwell shaded array,

$$\bar{a}_n = 0.42 - 0.50 \cos\frac{2\pi n}{N+1} + 0.08 \cos\frac{4\pi n}{N+1} . \tag{44}$$

The coefficients a_n are then defined to be

$$a_n = \bar{a}_n / Norm , \tag{45}$$

where

$$Norm = \sum_{n=1}^{N} \bar{a}_n \tag{46}$$

is a normalization constant.

7.3.2 Discrete Beamformers

In RANDI 3.1, the beam response due to shipping noise for a receiver array can be computed using either a coherent or an incoherent beamformer. The DFT coherent beamformer is defined by

$$B_{Ships,\,b} = \left| \sum_{n=1}^{N} a_n P_{Ships,\,n} \exp\left(i2\pi f \Delta\tau_{n,\,b}\right) \right|^2 , \tag{47}$$

where $B_{Ships,b}$ is the beam noise power due to shipping on beam b, $P_{Ships,n}$ is the total complex pressure at hydrophone n due to all ships, a_n is a shading coefficient, and $\Delta\tau_{n,b}$ is the time delay for hydrophone n used to form beam b.

The DFT incoherent beamforming is computed by

$$B_{Ships,\,b} = \sum_{s=1}^{Ships} \left| \sum_{n=1}^{N} a_n P_{s,\,n} \exp\left(i2\pi f \Delta\tau_{n,\,b}\right) \right|^2 , \tag{48}$$

where $P_{s,n}$ is the complex pressure at hydrophone n due to ship s.

For a line array with phones spaced a distance d apart, the time delay $\Delta\tau_{n,b}$ is given by

$$\Delta\tau_{n,b} = nd \cos \theta_b / c \tag{49}$$

and the beams are cosine spaced as described in Sec. 7.2.1, where B is the number of beams.

An FFT beamformer is also available in RANDI 3.1. The output power for beam m, $m = 1, 2, \ldots, N$, of the FFT beamformer is given by

$$B_{Ships,\,m} = \left| \sum_{n=1}^{N} a_n P_{Ships,\,n} (-1)^{n-1} \exp\left[-i2\pi(n-1)(m-1)/N\right] \right|^2 . \tag{50}$$

The FFT and the DFT beamformers will produce identical results for the special case when $B = N$ and the receiver array elements are half-wavelength spaced. At frequencies below the design frequency of the receiver array, the FFT beamformer forms virtual beams corresponding to beams with time delays larger than necessary to form an endfire beam. Berrou and Wagstaff (1982) have shown that virtual beams can be useful in tow system analysis. In general, the beams for the FFT beamformer point in directions which satisfy

$$\cos \theta_m = (f_d/f)\ [1 - 2(m-1)/N]. \tag{51}$$

Note that the beam directions for the FFT beamformer depend upon frequency. Also, the FFT algorithm used in the beamformer requires that N be a power of 2.

7.4 Array Response to Wind Noise

In contrast to shipping noise, wind noise is a random process. Local wind noise is computed using the Kuperman-Ingenito model (Sec. 5.0), which is range independent. An infinite layer of sources is located just below the surface and the bottom is layered. Both discrete (normal modes)

and continuous spectra are obtained. The wind model output is a cross-spectral density matrix, which is used in beamforming.

The beam outputs due to wind noise are determined by

$$B_{Wind,b} = \sum_{n=1}^{N} a_n^2 C_{Wind,nm} + 2 \sum_{n>m} a_n a_m \mathrm{Re}\left[C_{Wind,nm} e^{i2\pi f(n-m)\Delta\tau_b}\right], \tag{52}$$

where $C_{Wind,mn}$ is the cross-spectral density matrix due to wind noise at each element of the receiver array and

$$\Delta\tau_b = d \cos \theta_b / c \tag{53}$$

is the inner hydrophone time delay required to steer a beam in direction θ_b.

7.5 Array Response to Self Noise

In RANDI 3.1, there is an option to compute self noise, which consists of system noise and flow noise. Both of these components to the total noise field are described in terms of cross-spectral density matrices.

7.5.1 System Noise

The effect of system noise on beamforming is included in RANDI 3.1 by specifying the receiver array cross-spectral density matrix due to system noise. The elements in this cross-spectral density matrix are assumed to be of the form

$$C_{System,mn} = L_{System} \ \mathrm{sinc}[\pi md/D] , \tag{54}$$

where L_{System} is the omnidirectional system noise at the hydrophone level, d is hydrophone spacing, and D is a user-specified correlation length. This approach allows the user great flexibility in characterizing system noise. For $d/D >> 1$, system noise is effectively uncorrelated from hydrophone to hydrophone. For $d/D << 1$, system noise is correlated from hydrophone to hydrophone with the amount of correlation defined by the sinc function. Given the cross-spectral density matrix $C_{System,mn}$ and the desired steering direction θ_b, the beam output for system noise is given by

$$B_{System,b} = L_{System} \sum_{n=1}^{N} a_n^2 + 2 \sum_{n>m} a_n a_m C_{System,mn} \cos[2\pi f m \Delta\tau_b], \tag{55}$$

where $\Delta\tau_b$ is the inner hydrophone time delay required to steer a beam in direction θ_b, measured with respect to the receiver array axis.

7.5.2 Flow Noise

Flow noise (Bradley and Wagstaff 1991) in RANDI 3.1 is based on empirical data. Flow noise is assumed to produce a cross-spectral density matrix $C_{Flow,mn}$ for the receiver array of the form

$$C_{Flow,mn} = L_{Flow} \ (f/f_d)\delta_{mn} , \tag{56}$$

where f is the frequency, f_d is the design frequency of the receiver array, L_{Flow} is the omnidirectional flow noise at the hydrophone level, and δ_{mn} is the Kronecker delta function.

Beam output levels for either the FFT or DFT beamformers due to flow noise are independent of steering direction and are specified by

$$B_{Flow,b} = L_{Flow}(f/f_d) \sum_{n=1}^{N} a_n^2 \,. \tag{57}$$

The hydrophone flow noise level L_{Flow} depends upon the frequency and the tow speed. It is interpolated from the empirical data for frequencies in the range of 10 to 340 Hz and tow speeds in the range 5 to 18 kt. The flow noise formulation is not valid for $Nf/f_d < 1$.

At a frequency of 30 Hz, an array with 64 elements spaced 15 m apart results in omnidirectional flow noise levels as shown in Fig. 19 for the allowable range of tow speeds. At high tow speeds, flow noise can easily overwhelm the receiver array.

7.6 Combined Array Response

Shipping, wind, system, and flow noise are effectively independent sources of noise. By incoherently combining model predictions of the array response to these four noise sources, the total response can be estimated. For both DFT and FFT beamformers, this combination is performed at the beam output level. The result for a particular beam is simply

$$B_{Array,b} = B_{Ship,b} + B_{Wind,b} + B_{System,b} + B_{Flow,b} \,. \tag{58}$$

The incoherent DFT beamformer was used to beamform the received noise from the East China Sea example described earlier. Figures 20, 21, and 22 give the beam noise results from the rigorous, radial accumulation, and high-resolution radial accumulation shipping propagation methods, respectively. The three results are plotted on the same scale for ease of comparison. The beam noise includes the shipping noise field (shown in Figs. 9, 10, and 11), as well as noise from a 10-kt wind. Beam noise results using the radial methods compare very well with results from the rigorous method. The high-resolution radial accumulation method is only slightly different from the radial accumulation method.

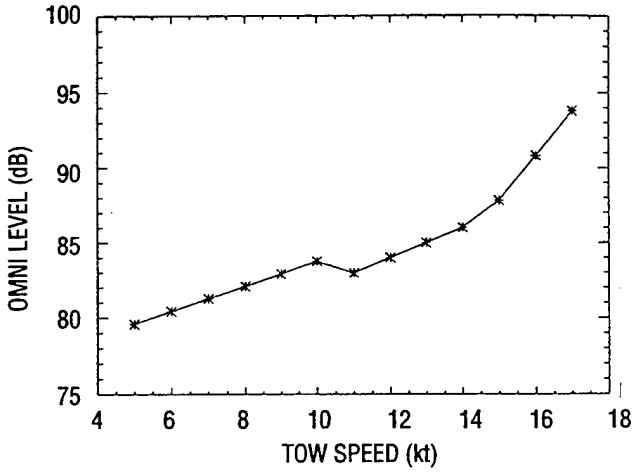

Fig. 19 — Example of omnidirectional flow noise levels vs. tow-ship speed for 30 Hz using a 64-element horizontal array with 15-m spacing

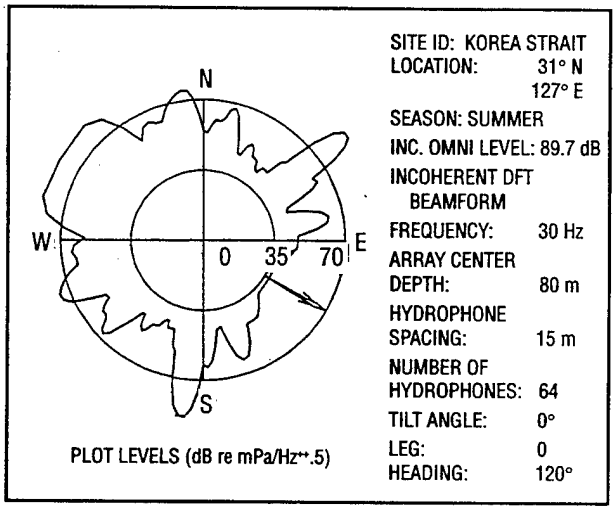

Fig. 20 — DFT beam noise with incoherent processing for the East China Sea example using the rigorous propagation method for ships

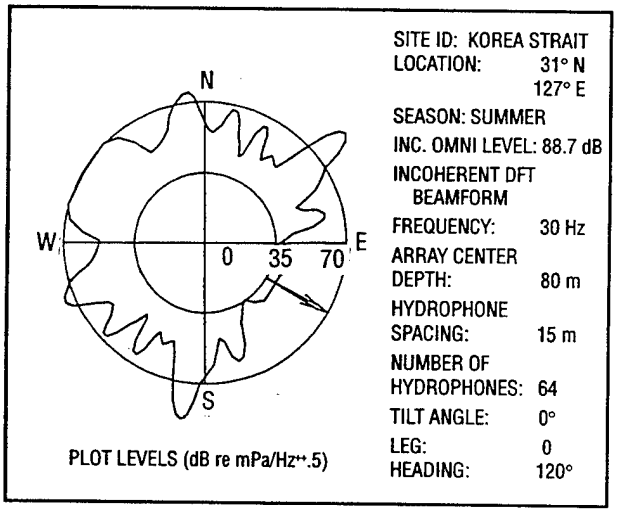

Fig. 21 — DFT beam noise with incoherent processing for the East China Sea example using the radial accumulation propagation method for ships

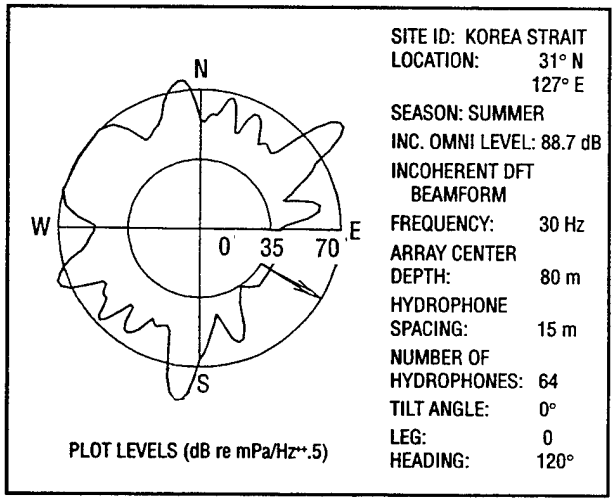

Fig. 22 — DFT beam noise with incoherent processing for the East China Sea example using the high-resolution radial accumulation propagation method for ships

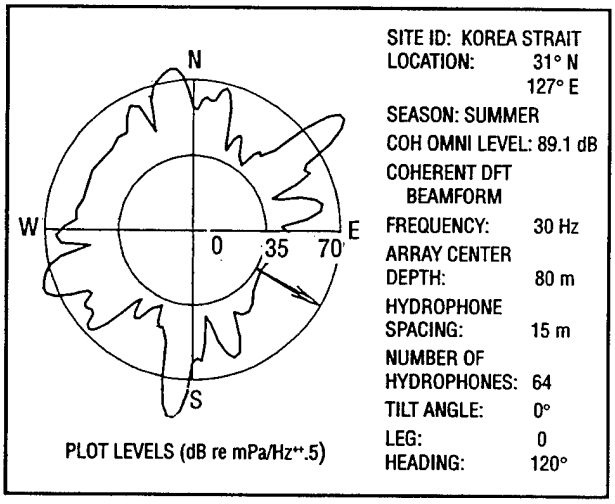

Fig. 23 — DFT beam noise with coherent processing for the East China Sea example using the high-resolution radial accumulation propagation method for ships

The coherent beam noise for the rigorous propagation method is shown in Fig. 23. Beam noise levels near endfire are somewhat suppressed when coherent processing is used instead of incoherent processing (compare to Fig. 20). Coherent processing may not be appropriate for the radial propagation methods since phase information is either not included or only approximated for individual ships.

The coherent and incoherent omnidirectional levels are calculated for each hydrophone in the array. The omnidirectional level for the array as a whole is taken to be the median of the hydrophone levels in decibels. The incoherent omnidirectional level compares favorably for the different propagation methods: 89.7 dB for the rigorous method versus 88.7 dB for the radial methods. The coherent omni-directional levels are equivalent for the rigorous and radial accumulation methods, and are equal to 89.1 dB.

8.0 ACKNOWLEDGMENTS

The authors thank Ronald A. Wagstaff of the Naval Research Laboratory and Michael Wooten of Planning Systems Incorporated for helpful discussions in the preparation of this report. This work was supported by the Office of Naval Research under the Coastal Ocean Sensors Project number 71-5354-B5, Program Element Number 0602435N, Program Manager Edward Chaika.

9.0 REFERENCES

Barnes, A. E., personal communication, 1995.

Berrou, J. L. and R. A. Wagstaff, "Virtual Beams from an FFT Beamformer and Their Use to Assess the Quality of a Towed-Array System," Proceedings of the ICASSP 82, IEEE International Conference on Acoustics, Speech, and Signal Processing, Vol. 2, 1982.

Bradley, M. R. and R. A. Wagstaff, "Flow Noise Modifications to RANDI-II," Technical Report TR-S025173, Planning Systems Inc., Slidell, LA, 1991.

Breeding, J. E., Jr., L. A. Pflug, M. Bradley, M. Hebert, and M. Wooten, "RANDI 3.1 Users Guide," NRL/MR/7176--94-7552, Naval Research Laboratory, Stennis Space Center, MS, 1994.

Collins, M. D., "FEPE Users Guide," NORDA Technical Note 365, Naval Research Laboratory, Stennis Space Center, MS, 1988.

Collins, M. D., "Applications and Time-Domain Solution of Higher-Order Parabolic Equations in Underwater Acoustics," *J. Acoust. Soc. Am.* **86**, 1097–1102 (1989).

Crout, R. L., "High Resolution Shallow Water Data Base Report," Technical Report TR-S446182, Planning Systems Inc., Slidell, LA, 1991.

Etter, P. C., *Underwater Acoustic Modeling* (Elsevier Science Publishers, Ltd., London, England, 1991).

Felizardo, F. C. and W. K. Melville, "Correlations Between Ambient Noise and the Ocean Surface Wave Field," *J. Phys. Oceanography* **25**, 513–532 (1995).

Hamilton, E. L., "Geoacoustic Modeling of the Sea Floor," *J. Acoust. Soc. Am.* **68**, 1313–1340 (1980).

Hamson, R. M., "The Theoretical Responses of Vertical and Horizontal Line Arrays to Wind Induced Noise in Shallow Water," *J. Acoust. Soc. Am.* **78**, 1702–1712 (1985).

Hamson, R. M. and R. A. Wagstaff, "An Ambient Noise Model that Includes Coherent Hydrophone Summation for Sonar System Performance in Shallow Water," Report SR-70, SACLANTCEN, LaSpezia, Italy, 1983.

Hardin, R. H. and F. D. Tappert, "Applications of the Split-Step Fourier Method to the Numerical Solution of Nonlinear and Variable Coefficient Wave Equations," *SIAM* Rev. **15**, 423 (1973).

Jensen, F. and M. Ferla, "SNAP—The SACLANTCEN Normal Mode Acoustic Propagation Model," SM-121, SACLANTCEN, LaSpezia, Italy, 1979.

Jensen, F. B., W. A. Kuperman, M. B. Porter, and H. Schmidt, *Computational Ocean Acoustics* (AIP Press, New York, NY, 1994).

Kuperman, W. A. and F. Ingenito, "Spatial Correlation of Surface Generated Noise in a Stratified Ocean," *J. Acoust. Soc. Am.* **67**, 1988–1996 (1980).

Kutschale, H. W., "Rapid Computation by Wave Theory of Propagation Loss in the Arctic Ocean," CU-8-73, Columbia University, New York, NY, 1973.

Molinelli, E., A. Barnes, J. Boyd, E. Weitzner, and E. Brosius, "The HITS Update Process and HITS III," Technical Report 446433, AEAS Report 90-107, Planning Systems Inc., Slidell, LA, 1990.

Naval Oceanographic Office, "Data Base Description for Digital Bathymetric Data Base Confidential (DBDBC)," OAML-DBD-17A, Stennis Space Center, MS, 1987.

Naval Oceanographic Office, "Data Base Description for Historical Wind Speed (HWS)," OAML-DBD-13B, Stennis Space Center, MS, 1989.

Naval Oceanographic Office, "Data Base Description for Low-Frequency Bottom Loss (LFBL)," OAML-DBD-12B, Stennis Space Center, MS, 1990a.

Naval Oceanographic Office, "Data Base Description for Master Generalized Digital Environmental Model (GDEM) Version 3.0," OAML-DBD-19B, Stennis Space Center, MS, 1990b.

Naval Oceanographic Office, "Data Base Description for Historical Temporal Shipping 3.0," OAML-DBD-43, Stennis Space Center, MS, 1993.

Ross, D., *Mechanics of Underwater Noise* (Peninsula Publishing, Los Altos, CA, 1987).

Spofford, C. W., R. R. Greene, and J. B. Hersey, "The Estimation of Geoacoustic Ocean Sediment Parameters from Measured Bottom Loss Data," SAI-83-879-WA, Science Applications International Corporation, San Diego, CA, 1983.

Tappert, F. D. and R. H. Hardin, "Computer Simulation of Long-Range Ocean Acoustic Propagation Using the Parabolic Equation Method," Proceedings of the 8th International Congress on Acoustics, Vol. 2, 1974, pp. 452.

Thomson, D. J. and N. R. Chapman, "A Wide-Angle Split-Step Algorithm for the Parabolic Equation," *J. Acoust. Soc. Am.* **74**, 1848–1854 (1983).

Wagstaff, R. A., "Low-Frequency Ambient Noise in the Deep Sound Channel—The Missing Component," *J. Acoust. Soc. Am.* **69**, 1009–1014 (1981).

Wilson, J. H., "Wind-Generated Noise Modeling," *J. Acoust. Soc. Am.* **73**, 211–216 (1983).